OPTIMUM SPACING BETWEEN VERTICAL, PARALLEL HEAT GENERATING BOARDS COOLED BY NATURAL CONVECTION IN A FIXED VOLUME

A THESIS SUBMITTED TO
THE GRADUATE SCHOOL OF NATURAL AND APPLIED SCIENCES
OF
MIDDLE EAST TECHNICAL UNIVERSITY

BY

SAMET SAYGAN

IN PARTIAL FULFILLMENT OF THE REQUIREMENTS
FOR
THE DEGREE OF MASTER OF SCIENCE
IN
MECHANICAL ENGINEERING

MAY 2014

Approval of the thesis:

OPTIMUM SPACING BETWEEN VERTICAL, PARALLEL HEAT GENERATING BOARDS COOLED BY NATURAL CONVECTION IN A FIXED VOLUME

submitted by **SAMET SAYGAN** in partial fulfillment of the requirements for the degree of **Master of Science in Mechanical Engineering Department, Middle East Technical University** by,

Prof. Dr. Canan Özgen _____
Dean, Graduate School of **Natural and Applied Sciences**

Prof. Dr. Suha Oral _____
Head of Department, **Mechanical Engineering**

Prof. Dr. Hafit Yüncü _____
Supervisor, **Mechanical Engineering Dept., METU**

Examining Committee Members:

Assoc. Prof. Dr. Cemil Yamalı _____
Mechanical Engineering Dept., METU

Prof. Dr. Hafit Yüncü _____
Mechanical Engineering Dept., METU

Assoc. Prof. Dr. Ahmet Yozgatlıgil _____
Mechanical Engineering Dept., METU

Asst. Prof. Dr. Özgür Bayer _____
Mechanical Engineering Dept., METU

Prof. Dr. Atilla Bıyıkoğlu _____
Mechanical Engineering Dept., Gazi University

Date: 26/05/2014

I hereby declare that all information in this document has been obtained and presented in accordance with academic rules and ethical conduct. I also declare that, as required by these rules and conduct, I have fully cited and referenced all material and results that are not original to this work.

Name, Last name : Samet Saygan

Signature :

ABSTRACT

OPTIMUM SPACING BETWEEN VERTICAL, PARALLEL HEAT GENERATING BOARDS COOLED BY NATURAL CONVECTION IN A FIXED VOLUME

Saygan, Samet
M.S., Department of Mechanical Engineering
Supervisor: Prof. Dr. Hafit Yüncü

May 2014, 81 pages

In this study, the effect of distance between vertical and parallel heat generating plates which are fixed in a given volume on the natural convection to the air between plates is investigated both numerically and experimentally.

The conservation equations which represent the constant property air flow in fixed and rectangular cross section channel are solved by the FloEFD software which used the Finite Volume Method and the SIMPLE algorithm. The maximum temperatures of plates are compared with the experimental results.

The optimum spacing in order to provide the maximum heat transfer to the air at given volume which plates are inserted and specified maximum temperature is determined.

By using the results of optimization, relations associated with the optimum spacing, which gives the maximum heat transfer rate, and width, height of the

plates and the kinematic and thermodynamic properties of air is derived. Those obtained relations are extended by using the results of studies in the literature which used plates in infinite width.

Keywords: Vertical and Parallel Boards, Natural Convection, Heat Generating Boards, Optimum Distance, Fixed Volume

ÖZ

DOĞAL KONVEKSİYON İLE SOĞUTULAN, DİK VE PARALEL BİR BİÇİMDE BELİRLİ BİR HACİME YERLEŞTİRİLEN ISI YAYAN PLAKALAR ARASINDAKİ OPTİMUM MESAFE

Saygan, Samet
Yüksek Lisans, Makine Mühendisliği Bölümü
Tez Yöneticisi: Prof. Dr. Hafit Yüncü

Mayıs 2014, 81 Sayfa

Bu çalışmada dik, paralel ve verilen bir hacme eşit aralıklarla yerleştirilmiş ısı yayan plakalar arasındaki mesafenin, aralarındaki havaya doğal taşınımla ısı transferine etkisi sayısal ve deneysel olarak incelenmiştir.

Dikdörtgen kesitli sabit kanaldaki ve sabit özellikli hava akışını temsil eden sakınım denklemleri sonlu hacim yöntemi ve SIMPLE algoritmasını kullanan FloEFD yazılımı ile çözülmüştür. Plakaların maksimum sıcaklıkları deneysel sonuçlarla karşılaştırılmıştır.

Dikdörtgen plakaların yerleştirildikleri verilen bir hacimde ve belirlenen maksimum sıcaklıkta havaya ısı transferinin maksimum olması için plakalar arasındaki optimum uzaklık belirlenmiştir.

Optimizasyon sonuçları kullanılarak en yüksek ısı transferini veren optimum uzaklık ile plakanın eni, boyu, uzunluğu ve havanın kinematik ve termo-dinamik

özellikleri cinsinden eş-ilişkiler türetilmiştir. Elde edilen eş-ilişkiler, literatürde genişliği sonsuz plakalar için geliştirilen sonuçlar göz önüne alınarak genelleştirilmiştir.

Anahtar Kelimeler: Dik ve Paralel Plakalar, Doğal Taşınım, Isı yayan Plakalar, Optimum Uzaklık, Sabit Hacim

To my family & my life

ACKNOWLEDGMENTS

First of all, I am very grateful to find a chance being a student of Prof. Dr. Hafit Yüncü during my Master of Science studies at Middle East Technical University, in terms of his guidance, inspiration, encourage, and invaluable help throughout the study.

I would like to express my gratitude to Mr. Serdar Terzi, my manager at Aselsan, for his valuable support during my Master of Science studies.

I acknowledge to TUBITAK (Turkish Scientific and Technical Research Council) owing to the two years financial support.

Finally, my special thanks goes to my family Şenay, Salih and Başak Saygan without whom none of my success would be possible; and my life, Bahar Bahtiyar, for being with me at all the times I need.

TABLE OF CONTENTS

LIST OF TABLES

TABLES

LIST OF FIGURES

FIGURES

NOMENCLATURE

C	Coefficient of optimum spacing equation
c_p	Specific heat [kJ/kgK]
FVM	Finite Volume Method
Gr	Grashof number (
g	Gravitational acceleration [m/s^2]
H	Height of the boards [mm]
k	Thermal conductivity [W/mK]
L	Length of the fixed volume [mm]
P	Pressure [Pa]
P'	Hydrostatic pressure [Pa]
P_∞	Atmospheric pressure [Pa]
$\overline{P}$	Dimensionless pressure
PCB	Printed Circuit Boards
Pr	Prandtl number
$\dot{Q}_{total}$	Total heat transfer from channel [W]
$\dot{q}''$	Heat flux [W/m^2]
R	Universal Gas Constant [J/kgK]
Ra	Rayleigh number
SIMPLE	Semi-Implicit Method for Pressure Linked Equations
S_u	Source function
S_p	Source function
s	Spacing between boards [mm]
s_{opt}	Optimum spacing between boards [mm]
T	Temperature [K]
T_∞	Ambient temperature [K]
$T_{w,max}$	Maximum wall temperature [K]

U_0	Reference velocity [m/s]
u	Velocity component in x-direction [m/s]
$\bar{u}$	Dimensionless x-velocity component
v	Velocity component in y-direction [m/s]
$\bar{v}$	Dimensionless y-velocity component
W	Width of the boards [mm]
w	Velocity component in z-direction [m/s]
$\bar{w}$	Dimensionless z-velocity component
x	Longitudinal coordinate along the height of the channel [m]
$\bar{x}$	Dimensionless longitudinal coordinate along the height of the channel
y	Transverse coordinate along the length of the channel [m]
$\bar{y}$	Dimensionless transverse coordinate along the length of the channel
z	Transverse coordinate along the width of the channel [m]
$\bar{z}$	Dimensionless transverse coordinate along the width of the channel
α	Thermal diffusivity [m^2/s]
ν	Kinematic viscosity [m^2/s]
ρ	Density of air [kg/m^3]
ρ_∞	Density of air at ambient temperature [kg/m^3]
μ	Dynamic viscosity [Pa.s]
β	Thermal expansion coefficient [K]
θ	Dimensionless temperature
Γ	Diffusion coefficient
Ø	Transport variable

CHAPTER 1

INTRODUCTION

Electronic devices are essential for our daily lives and also for many engineering fields such as health industry, defense industry etc. Specifically, televisions and cell phones in daily life; and Magnetic Resonance (MR) machines and military radio units in health and defense industry can be given as examples for applications of electronic devices. Moreover, not only the number of applications that electronics involved, but also the importance of electronic devices in our lives increases day by day.

All the electronic devices include printed circuit boards (PCBs) which are mechanical components including electrical links and electronic parts such as capacitors on it. These electronic parts generate heat naturally and sometimes these heat generating components may generate excessive amount of heat depending on their working conditions. That is to say, the more voltage on component, the more heat generates. Therefore, if the generated heat does not remove from the system, devices can fail and become inoperable. Some devices particularly in defense industry (e.g. military radio units, radars, etc.) have an essential importance for many aspects and failure of such devices can be troublesome. Thus, reliability of electronic components is very important. In other words, even in the worst circumstances such as in the warm ambient and the upper limit of the device's working capacity, the maximum temperature occurring in the electronic component should be less than its limit that those components can be able to work properly.

Reliability of the electronic components depends on various criteria; namely, architecture of electronic system, construction and density of components, operating conditions and the type of applications. In addition to these, one of the most important criteria that provides the successful operation of the device is the correct thermal management of the devices. Due to the fact that one can design complex and dense electronic system in optimal thermal management, this criterion may give an opportunity to make devices smaller without losing anything from its function [1].

There are several ways to remove generated heat from the devices. The most widely used ones are natural convection, forced convection, and two phase flows (e.g. heat pipes, and micro channels). As a working fluid, air is used in natural and forced convection whereas water and ammonia are used in heat pipes generally [2].

Procedures of removing generated heat mentioned above have both advantages and disadvantages. Firstly, heat pipes are devices that transport heat from a point to another point very quickly. Heat pipes are basically closed tubes; but apart from any other closed tubes, it includes a wick structure in it. This wick structure allows the liquid form of the working fluid to flow from cool side to the warm side. At the same time, hallow in the middle of the heat pipe enables to flow vapor form of the working fluid from warm side to the cool side [3]. This mechanism of the heat pipes has very large thermal conductivity in theory (100.000 W/mK). On the other hand, in practical, thermal conductivity is approximately 20.000 W/mK. Therefore, usage of heat pipes seems very logical to provide proper thermal management in electronic cooling. However, if the heat is not generated in specific points but spread over the device relatively equal, heat pipe usage may not be reasonable for proper thermal management. Secondly, in order to use heat pipes, one side of the heat pipe should be cooled rapidly. This rapid cooling is generally provided by fans and heat exchangers. In a condition of rapid cooling failure, the whole system might fail, as well. Lastly, there should be some spaces in order to place heat pipes in devices but the smallest heat pipe in the industry is

3 mm in diameter which is requires a considerable space in fact. However, due to the fact that one of the main aims in this industry has been getting devices as small as possible recently, using of heat pipes might be a disadvantage.

Another way of the thermal management of the system is the forced convection. In the forced convection, fluid motion which is generated by external devices (e.g. fans and blowers) is required for heat transfer between the heat source and the working fluid [4]. However, electronic devices are needed to be sealed against water of any liquid in case they are used in outdoors whereas there is no need for sealing in case of indoor usage. At the same time, this sealing condition is also valid for thermal management. That is to say, if the working fluid is water or any other liquid, sealing becomes vital; on the other hand, if air is used as a working fluid, sealing may be unnecessary. Therefore, air is the generally used working fluid in electronic cooling by forced convection because of its reliability and ease of use.

Also, capacity of cooling by forced convection is higher compared to natural convection. However, as mentioned above, forced convection is dependent on some external sources. If these external sources fail, devices get warmer quickly and fail ultimately. Moreover, constructing a system which is cooled by forced convection is more expensive than natural convection because external sources become necessary for the forced convection.

On the other hand, natural convection is the other most common way of thermal management. If fluids are heated at a constant pressure, they tend to expand and as a result of this tendency, the buoyancy effect occurs. The buoyancy effect is the driven force for natural convection. Therefore, natural convection starts spontaneously without requiring any external source since driven force of it arises naturally [5]. This procedure of cooling by natural convection makes it one of the cheapest procedures of thermal management. However, because the capacity of cooling by natural convection is decreased by its slowness of the fluid flow, it provides less effective cooling compared to forced convection. At that point,

geometry and orientation of the surface from which heat is removed becomes very crucial. For example, at the same temperature difference, rate of heat transfer from PCBs which is placed vertical is higher than horizontal ones. Also, the spacing between two PCBs affects the heat transfer rate substantially. Studies show that heat transfer rate increases at an increasing distance until it reaches its maximum level, and then it starts to decrease slightly with increasing distance until the effect of spacing becomes ineffective.

In the present thesis, analysis of two vertical and parallel plates will be analyzed by using FloEFD software under different heat generation rates for seven different aspect ratios of the plates between 15 and 0.5. Then, the results will be extent for an array of plates that are going to be fixed in a constant volume. In the meantime, an experimental setup will be established for a specified aspect ratio of 0.75 in order to verify the analysis results. At the end of the study, correlations will be suggested between the ratio of optimum spacing to height of the plates and the Gr x Pr number.

CHAPTER 2

LITERATURE SURVEY

Cooling systems by natural convection has been an important issue for engineers, particularly mechanical engineers, throughout the history. Researchers have tried to understand the mechanism of natural convection for different geometries in order to get proper cooling both experimentally and numerically. One of the most important geometries is vertical plates. Understanding the physics of natural convection from a vertical plate constitutes the basis of other geometries such as fins. In the literature, natural convection from vertical plates has been investigated in several approaches. The important approach on this issue is the boundary condition at heated walls. Literature review revealed that some studies use constant wall temperature case whereas others use constant heat flux case as a boundary condition. Studies have conducted in 2D or 3D computational domain either experimentally or numerically; or both experimentally and numerically.

As mentioned above, when investigating natural convection between vertical and parallel plates, two different boundary conditions can be defined at walls. These boundary conditions are constant wall temperature and constant heat flux. For instance, constant wall temperature case as a boundary condition was studied in [6], [7], [8], [9], [10], and [11]. On the other hand, [12], [13], and [14] have used constant heat flux case as a boundary condition at walls. In addition to these, there are some studies that conducted both constant wall temperature and constant heat flux cases [15] and [16]. Also, when solving natural convection problems, investigations can be conducted in two ways which are numerically and experimentally.

For constant wall temperature, [6] and [9] have studied numerically and [7], [8] and [10] have studied experimentally. Moreover, [11] has been studied both numerically and experimentally. One of the oldest studies on natural convection between two vertical plates has been conducted by Bodoia and Osterle [6] numerically. First of all, they have checked the possibility of fully developed flow between two parallel and vertical plates under natural convection and it has been found that fully developed flow between two plates under natural convection is almost impossible when the working fluid is air (Pr = 0.7). For instance, in a case that the temperature difference between the wall and the ambient is 1°C and the spacing between two plates equals to 0.1 ft.; the required height for fully developed flow would be approximately 10^3 ft. For this reason, that study was the first in terms of investigating the heat transfer and flow characteristics of channels which are shorter than the development height. The most important outcome of [6] was the mathematical relation between Nu and Gr numbers showed in equation (2.1). Accordingly, Levy [9] has also investigated the optimum spacing between vertical plates under natural convection in order to get minimum temperature difference between plates and the ambient. It has been found in this study that the ratio of two optimum spacing in case of maximum heat transfer rate and the minimum temperature are proportional to the ratio of multiplication of Gr, Pr and the ratio of spacing to the length of the plate in the order of 0.25. It is noteworthy that outcomes of both [6] and [9] are in parallel with each other. In addition to these numerical studies, Levy, Eichen, Cintani, & Shaw [10] have verified the results of [6] and [9] experimentally. For the experiments that conducted in [10], arrays of four and six aluminum plates have been used. The dimension of plates was 305 mm, 381 mm, 6.35 mm in width, height and thickness respectively. The spacing between the plates has changed between 6.25 and 25.4 mm. Results of this study showed that experimental and numerical results are very close to each other. The difference between numerical and experimental results has occurred when the dimensionless number is low. This is because of some assumptions. For example, in the numerical approach, constant property flow has been used and properties have been calculated at the mean temperature. However, for low values, flow has become thermally developed very

quickly. Therefore, it can be stated that properties at wall temperature may give more suitable results when compared to experiments [10].

$$Nu(\Pr Gr)^{-1/4} = f(\Pr) \tag{2.1}$$

There are three important experimental studies which were conducted on the natural convection between two parallel plates for constant wall temperature in different aspects. Sparrow and Bahrami [7] have aimed to examine the effects of lateral edges on convective heat transfer performance. Azevedo and Sparrow [8] have examined the convective heat transfer characteristics between the plates which were oriented in three different angles (0°, 30°, 45°). On the other hand, Ledezma and Bejan [11] have used the array of staggered vertical plates under the natural convection cooling both experimentally and numerically. Sparrow and Bahrami [7] have conducted their experiments in three different orientations. In the first orientation, there were no obstacles to prevent air flow from ambient. In the second one, air flow from one of the lateral edges was prevented. Lastly, in the third orientation, there was no air flow from the lateral edges. Sparrow and Bahrami [7] have concluded that flow characteristics were different for closed lateral edges as a third orientation compared to the first and the second one. When lateral edges were closed, chimney effect became very important on heat transfer case. It was found in [7] that if one of the lateral edges of the channel is closed, heat transfer characteristic was affected 15% for lower $(s/H)xRa$ numbers. This effect increased to 30% when both lateral edges had been closed. However, for higher $(s/H)xRa$ numbers $\left((s/H)xRa > 10\right)$ closed lateral edges did not affect the heat transfer characteristics.

As mentioned above, Azevedo and Sparrow [8] have studied the problem in different aspects. In their experiments, plates were placed in three different angles (0°, 30°, 45°) and the convective heat transfer characteristics between those plates were examined experimentally. The important result which is in the scope of this thesis was the vertical case (i.e. the inclination angle equals to 0°); correlations were found as in equations (2.2) and (2.3).

For both walls are heated:

$$Nu_s = 0.675\left[\left(s/H\right)Ra_s\right]^{0.25} \tag{2.2}$$

For one of the walls is heated and the other one is insulated:

$$Nu_s = 0.642\left[\left(s/H\right)Ra_s\right]^{0.25} \tag{2.3}$$

Furthermore, a fixed volume was used to place staggered vertical plates in [11]. In the same study, Pr number of the working fluid was fixed at 0.72 (i.e. air). Ra number which was calculated by using height of the plates was changed between 10^3 and 10^6. In this study, it was found that there was an optimal spacing between heated vertical plates in order to get maximum convective heat transfer rate. According to Ledezma and Bejan [11], optimum spacing between vertical plates was formulated as showed in the equation (2.4).

$$\frac{s_{opt}}{H} \cong 2.3Ra_H^{-1/4} \tag{2.4}$$

It is noteworthy that there is consistency between equation (2.2), (2.3) and (2.4). For all the equations, effect of Ra number is in the order of 0.25.

As mentioned above, [12] and [13] have used constant heat flux case as a boundary condition in walls. Moreover, both uniform heat flux and constant wall temperature case have been used as boundary conditions in [15] and [16]. In the experimental study of Wirtz and Stutzman [12], plates which were square in shape, dimensions were 303.2mm x 303.2mm, and the thickness was 3.4 mm. On the other hand, Ramanathan and Kumar [13] have extended the studies on natural convection between two vertical and parallel plates to a large enclosure. Also, they have repeated their solutions for different Pr number and aspect ratios which were defined the ratio of spacing between plates to the height of the plate. Wirtz

and Stutzman [12] have investigated four different spacing between 7.94mm and 17.78mm; and air was the working fluid in that experiment. That is to say, Pr number has been considered as constant in that study. Also, those experiments have been conducted for different heat flux values. As a result of the study of Wirtz and Stutzman [12], an important correlation has been found for Nu number for two vertical plates which were cooled by natural convection as shown in equation (2.7). In addition to [12], Ramanathan and Kumar [13] have found that when the aspect ratio is low, the maximum temperature occurs at the midsection of the vertical plate. The possible reason of this could be the fact that the situation occurs due to heat conduction in vertical direction. It should be emphasized that conduction in vertical direction is not effective for higher aspect ratios significantly [13]. For high Ra numbers, the maximum temperature occurs at the top of the plates. Ramanathan and Kumar [13] have suggested certain correlations for maximum temperature and for Nu number. These correlations can be listed as:

For $1 \leq H/s \leq 15$ and $10 \leq Ra \leq 3x10^5$ and Pr = 0.7

$$T_{\max} = \left\{ \left[\frac{\left(H/s \right)^2}{5} + \frac{\left(H/s \right)^4}{15} \right]^{-1.1} + 0.0122 Ra^{1.1} (1 + 0.0156 Ra^{0.9})^{-0.75} \right\}^{-0.4} \tag{2.5}$$

$$Nu = \left\{ \frac{185}{H/s} + (23 Ra^{-1.3} + 0.5 Ra^{-0.6})^{-1.25} \right\}^{0.2} \tag{2.6}$$

$$Nu(L) = \frac{0.042 Ra_T}{\left[1 + 7 \times 10^{-5} Ra_T^{2.25} \right]^{0.333}} \tag{2.7}$$

Furthermore, the results of [12] and [13] were consistent with each other in 25% deviation. The difference between the two results has arisen from the experimental errors and the assumptions in numerical solution. It is also noteworthy that, it is almost impossible to setup an experiment which is identical

to mathematical model. Therefore, 25% deviation between results of two different studies can be interpreted as acceptable.

Also Bejan and Lee [14] have studied the natural convection cooling for array of vertical heat generating boards, forced convection cooling for array of horizontal heat generating boards and forced convection cooling of horizontal heat generating board in a channel. For the natural convection cooling for array of vertical heat generating boards case, they found the relation for optimum spacing (equation 2.8) when the ratio of board width to the board height (W/H) approaches to infinity.

$$\frac{D_{opt}}{H} \cong 2.3\left[\frac{g\beta(T_{\max}-T_{\infty})H^{3}}{\alpha\nu}\right]^{-1/4} \tag{2.8}$$

In the study of Anand, Kim and Fletcher [15], both uniform heat flux case and uniform surface temperature case for two vertical plates under natural convection have been examined. In the [15], the effect of Gr number on the convective cooling has been studied mostly. It was found that as the ratio of spacing between vertical plates to the length of the plates decreases, Nu number increases. The reason of this is that the increment can be explained by chimney effect. Also, the chimney effect is more effective when the Gr number is large. Decreasing continuously of the ratio of spacing to the length means decreasing of the spacing between plates; and ultimately, the boundary layers of the plates touches to each other. At that moment, chimney effect disappears and Nu number decreases. This result is valid for both uniform heat flux and uniform wall temperature cases. Also, from the results of this investigation, it can be stated that the effect of asymmetric heating parameter on the optimum spacing is very low. The results this study were limited for the case of Gr number is less than 10^5; however, results also show that as the Gr number increases, the optimum spacing decreases. Therefore, the optimum spacing for Gr number which is higher than the 10^5 should be lower than the optimum spacing value when Gr = 10^5 in this study [15]. On the other hand, Bar-Cohen and Rohsenow [16] have made an extensive

research investigating the convective heat transfer characteristics of two vertical plates and also have extended to an array of plates. The research was extensive because they have considered both constant heat flux and constant wall temperature cases for both symmetric and asymmetric heating conditions. Forward integral formulation method has been used in order to derive optimum spacing formulation. Specifically for symmetric isothermal (i.e. constant wall temperature) plates, optimum spacing has been found as:

$$s_{opt} = \frac{2.714}{P^{1/4}} \tag{2.9}$$

where P is plate/air parameter and P is defined as:

$$P = \frac{C_p \rho^2 g \beta \Delta T_0}{\mu k H} \tag{2.10}$$

For symmetric plates under constant heat flux condition, optimum spacing is found as:

$$s_{opt} = 1.472 R^{-0.2} \tag{2.11}$$

where R is defined as:

$$R = \frac{C_p \rho^2 g \beta \dot{q}''}{\mu H k^2} \tag{2.12}$$

Qing, Suizheng, Guanghui, Wenxi, and Zhonghao [17] have been investigated the natural convection in vertical and rectangular channels. Their study was experimental and the aspect ratio of it was large. They found that the Nu number was a function of Ra number. The coefficient and the exponent of the Ra number in the correlations were different for different Ra number intervals.

Usage of fins in order to cool heat generating systems is used commonly in thermal management. The fins which are in rectangular shape and placed vertically on the systems can be considered as vertical plates in low width. Another difference between the fins and parallel plates is their lateral edges. If the fins are placed as in Fig. 2.1, then it can be stated that vertical plates in an array, which is one of lateral edges, is closed as mentioned in [7]. If they are placed as in Fig. 2.2, on the other hand, then the base is closed with an obstacle.

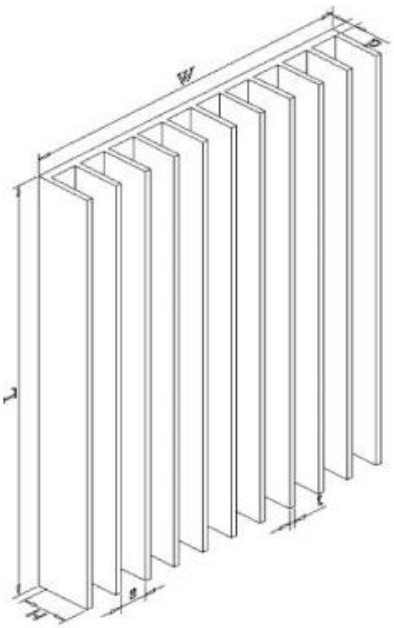

Fig. 2.1 Fins are in Vertical Base

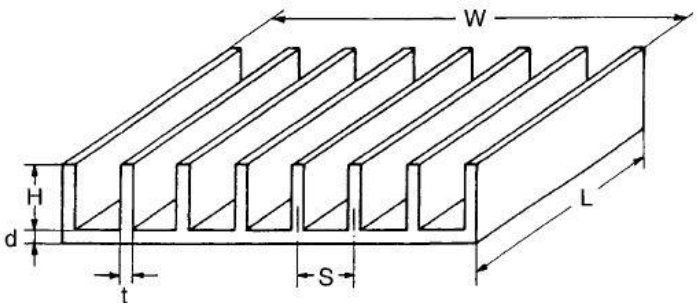

Fig. 2.2 Fins are in Horizontal Base

Three studies, [18], [19] and [20], which have been conducted about optimum spacing between fins in different orientations and in different heating conditions are discussed. Yüncü and Anbar [18] have investigated the heat transfer performance of horizontal rectangular fins, as shown in Fig. 2.2, under natural convection experimentally. On the other hand, Güvenç and Yüncü [19] and Yazıcıoğlu and Yüncü [20] have performed different experiments using vertical rectangular fins under the steady state natural convection in order to find the effects of geometric parameters, which are fin spacing, fin height, fin length, and base-to-ambient temperature difference on the performance of natural convection cooling from the fins. In the experimental study of Yüncü and Anbar [18], heat transfer performance of horizontal rectangular fins under natural convection has been conducted. In the experiments of that study, 15 different fin-array configurations have been tested at fixed length (100mm) and thickness (3mm) of the fins. On the other hand, fin height was changed between 6mm and 26mm, and also fin spacing was changed between 6.2mm and 83mm. 8 W to 50 W heaters were used in order to provide temperature difference between the base and the ambient. Yüncü and Anbar [18] have found that fin height, fin spacing and temperature differences between the fin base and surroundings are based on heat transfer rate from fins. It was also found that for fins in which height is large, heat transfer rate with temperature differences increases greater than the small height fins. At the same time, Yüncü and Anbar [18] have found that as temperature difference increases, heat transfer increases monotonously, as well. One of the important results, especially for the current thesis, was that the heat transfer rate increases with increasing fin spacing when fin height and temperature difference between fin base and surroundings are fixed. After heat transfer rate reaches a maximum value, then it starts to decrease with increasing fin spacing. When the heat transfer rate is in maximum level, the spacing of this point is called optimum fin spacing; and for many practical applications, this optimum spacing has an essential importance. Finally, it was found that for 26mm fins, the optimum spacing is 10.4mm; for 16mm fins, the optimum spacing is 11,6mm; and for 6mm fins, the optimum spacing is 19.5mm.

In the experiments of Güvenç and Yüncü [19], 15 different fin configurations have been used, as well, but in different orientation compared to [18]. In this study [19], fin length was 100 mm and fin thickness was 3 mm. Also, three different fin heights which were 5 mm, 15 mm and 25 mm, have been investigated. For those three different heights, there were five different fin spacing. Values of the spacing were 4.5 mm, 7.3 mm, 16 mm, 32.3 mm, and 58.75 mm. Furthermore, Yazıcıoğlu and Yüncü [20] have fixed the fin thickness to 3 mm. Whereas fin lengths were 250 mm and 340 mm which was different from [19]; and three different fin heights which were 5 mm, 15 mm and 25 mm were used in the experiments of this study [20]. Also, five different spacing were investigated in this study. Spacing started from 5.85 mm and it ended at 85 mm. Between 25 W and 125 W, five different heat inputs were applied to fin configurations. The major difference between [19] and [20] was that in the [20], two different fin lengths were conducted. Therefore, it can be concluded that [20] gives more generalizable results than [19]. In both [19] and [20], it was found that the heat transfer rate directly related to height of fins and the temperature difference between the base and the ambient. According to the common results of these two studies, if these two variables increase, then heat transfer rate also increases. One of the most important outcomes of these two studies is that for the fixed fin height and the fixed temperature difference between the base and the ambient, convective heat transfer rate increases with increasing spacing for a certain value and decreases with further increasing spacing. Unlike [20], Güvenç and Yüncü [19] have found that optimum spacing which maximizes the heat transfer rate from the fins approximately equals to 7 mm when fin heights changed between 5 mm and 25 mm; and fin length was 100 mm. On the other hand, Yazıcıoğlu and Yüncü [20] have found a correlation between optimum spacing and Ra number as shown in equation (2.12). It should be emphasized that again in this equation, optimum spacing is proportional to Ra number in the order of 0.25.

$$\frac{s_{opt}}{L} = 3.94 Ra_L^{-1/4} \tag{2.13}$$

CHAPTER 3

THEORY

3.1 COMPUTATIONAL DOMAIN

Fig. 3.1 illustrates the geometry of the electronic package. The model which is used in this thesis is composed of arrays of vertical and parallel channels. The lateral walls of the channels are insulated. The volume of the electronic package is fixed and its height, length, and width are H x L x W respectively. A sufficiently large number of parallel and vertical heat generating printed circuit boards are installed in the package in equal distances. Those parallel and vertical heat generating boards are cooled by natural convection of atmospheric air at uniform ambient temperature T_∞.

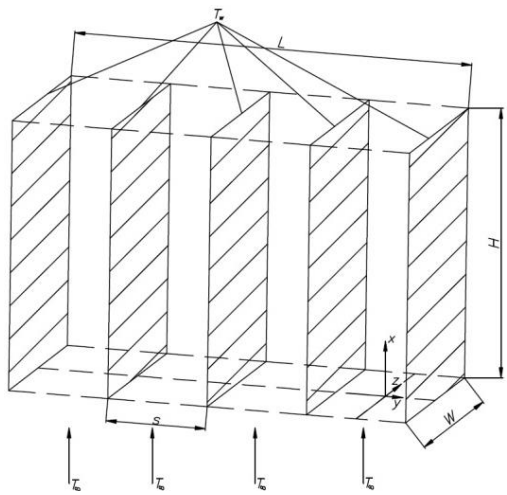

Figure 3.1: Geometry of the Electronic Package

Cold air at the ambient temperature T_∞ enters through the bottom of the package; then, it rises through the board to board channel, and exits through the upper opening. Parallel and vertical heat generating boards are kept at constant uniform heat flux.

In practice, several chip packages are distributed on the surface of the heat generating boards. In modeling, however, the effects of chip packages are neglected. The boards are flush-mounted and double sided. Heat is generated from the both surfaces of the printed circuit boards; and the flow of the atmospheric air is maintained by the buoyancy force. The maximum of the board temperature $T_{w.max}$ is set by electronic operational constraints.

The objective of the thesis is to find the optimum spacing (s_{opt}) between the heat generating boards in order to dissipate maximum heat transfer rate from the electronic package (H x L x W space). Numerical calculations for finding temperature distribution are performed for a single channel which is shown in Fig. 3.2. The height, length, and width of the single channel are H x L x s respectively. Numerical calculations are performed by the software which is named as FloEFD developed by Mentor Graphics. Details of this software are explained in Chapter 4. Then, the heat transfer rate from the single channel is determined numerically, the solution is extended to whole assembly which is shown in Fig. 3.1.

In order to verify the numerical solution of the assembly, solution of numerical code (software) for certain case is compared by the results of comprehensive experiments.

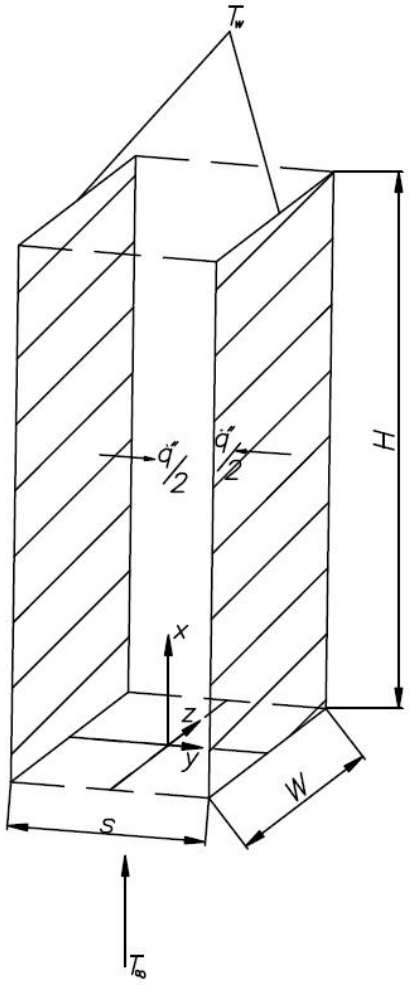

Figure 3.2: Schematic Representation of the Single Channel of the System

3.2 GOVERNING EQUATIONS

The continuity, momentum and energy equations are simplified by assuming:

- **a.** Air flow is steady and laminar
- **b.** Flow is incompressible (moderate velocity and temperature variation)
- **c.** Viscous dissipation is neglected

The gravity is taken in -x direction along the channel; and thickness of the plates is neglected. Also a hydrostatic pressure (P') is defined by as:

$$P' = P + \rho_\infty g x \tag{3.1}$$

In the light of these assumptions, governing equations can be written as:

Continuity equation:

$$\frac{\partial u}{\partial x} + \frac{\partial v}{\partial y} + \frac{\partial w}{\partial z} = 0 \tag{3.2}$$

Momentum equation in x-direction:

$$\rho(u\frac{\partial u}{\partial x} + v\frac{\partial u}{\partial y} + w\frac{\partial u}{\partial z}) = -\frac{\partial P}{\partial x} + \mu(\frac{\partial^2 u}{\partial x^2} + \frac{\partial^2 u}{\partial y^2} + \frac{\partial^2 u}{\partial z^2}) - \rho g \tag{3.3}$$

Momentum equation in y-direction:

$$\rho(u\frac{\partial v}{\partial x} + v\frac{\partial v}{\partial y} + w\frac{\partial v}{\partial z}) = -\frac{\partial P}{\partial y} + \mu(\frac{\partial^2 v}{\partial x^2} + \frac{\partial^2 v}{\partial y^2} + \frac{\partial^2 v}{\partial z^2}) \tag{3.4}$$

Momentum equation in z-direction:

$$\rho(u\frac{\partial w}{\partial x} + v\frac{\partial w}{\partial y} + w\frac{\partial w}{\partial z}) = -\frac{\partial P}{\partial z} + \mu(\frac{\partial^2 w}{\partial x^2} + \frac{\partial^2 w}{\partial y^2} + \frac{\partial^2 w}{\partial z^2}) \tag{3.5}$$

Energy equation:

$$u\frac{\partial T}{\partial x} + v\frac{\partial T}{\partial y} + w\frac{\partial T}{\partial z} = \alpha(\frac{\partial^2 T}{\partial x^2} + \frac{\partial^2 T}{\partial y^2} + \frac{\partial^2 T}{\partial z^2}) \tag{3.6}$$

u, v, and w are the velocity components of the flow field, where those are in x, y, z directions respectively. P is the pressure, ρ is the density, μ is the absolute

viscosity, and g is the gravitational acceleration which is in the –x direction. Note that the gravity term (ρg term) is only in the equation (3.3) because the body force is only in x-direction.

If hydrostatic pressure (equation (3.1)) is used in the momentum equations, then momentum equations from (3.3) to (3.5) become:

$$\rho(u\frac{\partial u}{\partial x}+v\frac{\partial u}{\partial y}+w\frac{\partial u}{\partial z})=-\frac{\partial P'}{\partial x}+\mu(\frac{\partial^2 u}{\partial x^2}+\frac{\partial^2 u}{\partial y^2}+\frac{\partial^2 u}{\partial z^2})-g(\rho-\rho_\infty) \tag{3.7}$$

$$\rho(u\frac{\partial v}{\partial x}+v\frac{\partial v}{\partial y}+w\frac{\partial v}{\partial z})=-\frac{\partial P'}{\partial y}+\mu(\frac{\partial^2 v}{\partial x^2}+\frac{\partial^2 v}{\partial y^2}+\frac{\partial^2 v}{\partial z^2}) \tag{3.8}$$

$$\rho(u\frac{\partial w}{\partial x}+v\frac{\partial w}{\partial y}+w\frac{\partial w}{\partial z})=-\frac{\partial P'}{\partial x}+\mu(\frac{\partial^2 w}{\partial x^2}+\frac{\partial^2 w}{\partial y^2}+\frac{\partial^2 w}{\partial z^2}) \tag{3.9}$$

Then equation (3.7) can be written as:

$$\rho(u\frac{\partial u}{\partial x}+v\frac{\partial u}{\partial y}+w\frac{\partial u}{\partial z})=-\frac{\partial P'}{\partial x}+\mu(\frac{\partial^2 u}{\partial x^2}+\frac{\partial^2 u}{\partial y^2}+\frac{\partial^2 u}{\partial z^2})+g(\rho_\infty-\rho) \tag{3.10}$$

Assuming the air is ideal gas; and based on ideal gas model for all level of x, it can be written as:

$$P=\rho RT \tag{3.11}$$

$$\rho=\frac{P_\infty/R}{T} \tag{3.12}$$

$$\rho_\infty=\frac{P_\infty/R}{T_\infty} \tag{3.13}$$

Rearranging the equations (3.12) and (3.13) gives

$$\rho - \rho_\infty = \rho(1 - \frac{T}{T_\infty}) \quad \Rightarrow \frac{\rho_\infty - \rho}{\rho_\infty}(1 - \frac{\rho_\infty - \rho}{\rho_\infty})^{-1} = \frac{T - T_\infty}{T_\infty} \tag{3.14}$$

in the limit $(T - T_\infty) << T_\infty$

$$\rho \cong \rho_\infty \left[1 - \frac{1}{T_\infty}(T - T_\infty) + ... \right] \tag{3.15}$$

From the above equation, it can be concluded that the density decreases slightly below ρ_∞ as the local absolute temperature increases slightly above the reservoir temperature T_∞ [21]. It can be written as:

$$\rho \cong \rho_\infty \left[1 - \beta(T - T_\infty) + ... \right] \tag{3.16}$$

where β is the volume expansion coefficient at constant pressure.

$$\beta = -\frac{1}{\rho}\left(\frac{\partial \rho}{\partial T}\right)_P \tag{3.17}$$

It is assumed that the dimensionless product $\beta(T - T_\infty)$ is considerably smaller than unity and by using Boussinesq approximation, the inertia terms are going to multiplied by the dominant term ρ_∞ which is constant. As a result, x-momentum equation (3.10) becomes:

$$u\frac{\partial u}{\partial x} + v\frac{\partial u}{\partial y} + w\frac{\partial u}{\partial z} = -\frac{1}{\rho}\frac{\partial P'}{\partial x} + \nu(\frac{\partial^2 u}{\partial x^2} + \frac{\partial^2 u}{\partial y^2} + \frac{\partial^2 u}{\partial z^2}) + g\beta(T - T_\infty) \tag{3.18}$$

In order to make governing equations dimensionless, some dimensionless parameters are defined as follows:

$$\bar{x} = \frac{x}{H} \tag{3.19a}$$

$$\bar{y} = \frac{y}{H} \tag{3.19b}$$

$$\bar{z} = \frac{z}{H} \tag{3.19c}$$

$$\bar{u} = \frac{u}{U_0} \tag{3.19d}$$

$$\bar{v} = \frac{v}{U_0} \tag{3.19e}$$

$$\bar{w} = \frac{w}{U_0} \tag{3.19f}$$

$$\theta = \frac{T - T_\infty}{T_{w,\max} - T_\infty} \tag{3.19g}$$

$$\bar{P} = \frac{P'}{\rho U_0{}^2} \tag{3.19h}$$

Then governing equations become as follows:

$$\frac{\partial \bar{u}}{\partial \bar{x}} + \frac{\partial \bar{v}}{\partial \bar{y}} + \frac{\partial \bar{w}}{\partial \bar{z}} = 0 \tag{3.20}$$

$$\bar{u}\frac{\partial \bar{u}}{\partial \bar{x}} + \bar{v}\frac{\partial \bar{u}}{\partial \bar{y}} + \bar{w}\frac{\partial \bar{u}}{\partial \bar{z}} = -\frac{\partial \bar{P}}{\partial \bar{x}} + \frac{g\beta(T_{w,\max} - T_\infty)H}{U_0{}^2}\theta + \frac{\nu}{HU_0}\nabla^2\bar{u} \tag{3.21}$$

$$\bar{u}\frac{\partial \bar{v}}{\partial \bar{x}}+\bar{v}\frac{\partial \bar{v}}{\partial \bar{y}}+\bar{w}\frac{\partial \bar{v}}{\partial \bar{z}}=-\frac{\partial \bar{P}}{\partial \bar{y}}+\frac{\nu}{HU_0}\nabla^2\bar{v} \tag{3.22}$$

$$\bar{u}\frac{\partial \bar{w}}{\partial \bar{x}}+\bar{v}\frac{\partial \bar{w}}{\partial \bar{y}}+\bar{w}\frac{\partial \bar{w}}{\partial \bar{z}}=-\frac{\partial \bar{P}}{\partial \bar{z}}+\frac{\nu}{HU_0}\nabla^2\bar{w} \tag{3.23}$$

$$\bar{u}\frac{\partial \theta}{\partial \bar{x}}+\bar{v}\frac{\partial \theta}{\partial \bar{y}}+\bar{w}\frac{\partial \theta}{\partial \bar{z}}=\frac{1}{\mathrm{Re}\,\mathrm{Pr}}\left(\frac{\partial^2\theta}{\partial \bar{x}^2}+\frac{\partial^2\theta}{\partial \bar{y}^2}+\frac{\partial^2\theta}{\partial \bar{z}^2}\right) \tag{3.24}$$

The dimensionless parameter in the first term on the right hand side of the equation (3.21) is the consequence of the buoyancy force. Since the reference velocity U_0 is arbitrary, it can be chosen in order to simplify the form of equation. It is convenient to choose U^2_0 as:

$$U_0{}^2 = g\beta(T_{w,\max}-T_\infty)H \tag{3.25}$$

Then the coefficient of the θ becomes unity after the simplification. The dimensionless parameter in the third term on the right hand side of the equation (3.21) and the second term on the right hand side of the equations (3.22) and (3.23) are the same. This dimensionless group becomes:

$$\frac{U_0 H}{\nu}=\left[\frac{g\beta(T_{w,\max}-T_\infty)H^3}{\nu^2}\right]^{1/2} \tag{3.26}$$

It is customary to define the square of the term U_0H/ν as Grashof number:

$$Gr_H=\frac{g\beta(T_{w,\max}-T_\infty)H^3}{\nu^2} \tag{3.27}$$

As a result, the term U_0H/ν is replaced by $Gr_H{}^{1/2}$.

Grashof number plays the same role in free convection as the Reynolds number plays in forced convection.

When the foregoing definition of the Grashof number is substituted into equations (3.21), (3.22), (3.23), and (3.24); then the governing equations are expressed as:

$$\frac{\partial \bar{u}}{\partial \bar{x}} + \frac{\partial \bar{v}}{\partial \bar{y}} + \frac{\partial \bar{w}}{\partial \bar{z}} = 0 \tag{3.28}$$

$$\bar{u}\frac{\partial \bar{u}}{\partial \bar{x}} + \bar{v}\frac{\partial \bar{u}}{\partial \bar{y}} + \bar{w}\frac{\partial \bar{u}}{\partial \bar{z}} = -\frac{\partial \bar{P}}{\partial \bar{x}} + \theta + \frac{1}{\sqrt{Gr}}\nabla^2 \bar{u} \tag{3.29}$$

$$\bar{u}\frac{\partial \bar{v}}{\partial \bar{x}} + \bar{v}\frac{\partial \bar{v}}{\partial \bar{y}} + \bar{w}\frac{\partial \bar{v}}{\partial \bar{z}} = -\frac{\partial \bar{P}}{\partial \bar{y}} + \frac{1}{\sqrt{Gr}}\nabla^2 \bar{v} \tag{3.30}$$

$$\bar{u}\frac{\partial \bar{w}}{\partial \bar{x}} + \bar{v}\frac{\partial \bar{w}}{\partial \bar{y}} + \bar{w}\frac{\partial \bar{w}}{\partial \bar{z}} = -\frac{\partial \bar{P}}{\partial \bar{z}} + \frac{1}{\sqrt{Gr}}\nabla^2 \bar{w} \tag{3.31}$$

$$\bar{u}\frac{\partial \theta}{\partial \bar{x}} + \bar{v}\frac{\partial \theta}{\partial \bar{y}} + \bar{w}\frac{\partial \theta}{\partial \bar{z}} = \frac{1}{\sqrt{Gr}\,\mathrm{Pr}}\nabla^2 \theta \tag{3.32}$$

3.3 BOUNDARY CONDITIONS

The governing differential equations are elliptic. For the solution of those equations, boundary conditions are required. In this section, boundary conditions at each boundary are defined and introduced separately. Because of the symmetrical nature of the computational domain in y and z directions, those directions are taken into account in the determination of the boundary conditions.

3.3.1 Boundary Condition at the Inlet $(\bar{x} = 0)$

At the inlet, velocities are assumed to be zero in all directions and the temperature of the air assumed to be equal to ambient temperature (T_∞). The non-dimensional forms of boundary conditions can be written as:

at $\bar{x} = 0$ & $\frac{s}{2H} \geq \bar{y} \geq 0$ & $\frac{W}{2H} \geq \bar{z} \geq 0$

$$\bar{u} = 0 \tag{3.33a}$$

$$\bar{v} = 0 \tag{3.33b}$$

$$\bar{w} = 0 \tag{3.33c}$$

$$\theta = 0 \quad (T = T_\infty) \tag{3.33d}$$

3.3.2 Boundary Condition at the Outlet $(\bar{x} = 1)$

At the outlet, since the parameter length (L) is sufficiently long, it is assumed that the change of velocity and temperature profiles with respect to x is zero. Boundary conditions can be listed in non-dimensional form as:

at $\bar{x} = 1$ & $\frac{s}{2H} \geq \bar{y} \geq 0$ & $\frac{W}{2H} \geq \bar{z} \geq 0$

$$\frac{\partial \bar{u}}{\partial \bar{x}} = 0 \tag{3.34a}$$

$$\frac{\partial \bar{v}}{\partial \bar{x}} = 0 \tag{3.34b}$$

$$\frac{\partial \overline{w}}{\partial \overline{x}} = 0 \tag{3.34c}$$

$$\frac{\partial \theta}{\partial \overline{x}} = 0 \tag{3.34d}$$

at $\overline{y} = \frac{s}{2H}$

$$\theta = 1 \quad (T = T_{w,\max}) \tag{3.34e}$$

3.3.3 Boundary Condition at y=0

At y= 0 (i.e. in the middle of two plates), the slope of x component of velocity and temperature with respect to y are zero. Also at this point, y and z components of the velocity equal to zero.

at $\overline{y} = 0$ & $1 \geq \overline{x} \geq 0$ & $\frac{W}{2H} \geq \overline{z} \geq 0$

$$\frac{\partial \overline{u}}{\partial \overline{y}} = 0 \tag{3.35a}$$

$$\overline{v} = 0 \tag{3.35b}$$

$$\overline{w} = 0 \tag{3.35c}$$

$$\frac{\partial \theta}{\partial \overline{y}} = 0 \tag{3.35d}$$

3.3.4 Boundary Condition at y=s/2

This boundary condition refers to the surface of the plates. Because of the no-slip assumption, all components of velocity are zero at the surface of the plates. On the other hand, multiplication of the slope of temperature change with respect to y axis by thermal conductivity of air equals to heat flux from the plates. The reason to take minus sign of the heat flux from the wall is because of the opposite direction of axis and the heat flux. This condition is the result of the constant heat flux condition at plates. The boundary conditions can be written in non-dimensional form as:

at $\bar{y} = \dfrac{s}{2H}$ & $1 \geq \bar{x} \geq 0$ & $\dfrac{W}{2H} \geq \bar{z} \geq 0$

$$\bar{u} = 0 \tag{3.36a}$$

$$\bar{v} = 0 \tag{3.36b}$$

$$\bar{w} = 0 \tag{3.36c}$$

$$k\left(-\frac{\partial T}{\partial y}\right) = -\frac{\dot{q}''}{2} \tag{3.36d}$$

The non-dimensional form of the equation (3.36d) is:

$$\frac{\partial \theta}{\partial \bar{y}} = \frac{\dot{q}''H}{2k(T_{w,\max} - T_{\infty})} \tag{3.37}$$

3.3.5 Boundary Condition at z=0

This condition refers to the mid-plane of two lateral edges which are assumed to be insulated. As same as in the boundary condition at y= 0; also in this region, the slope x component of velocity and temperature with respect to z axis equal to zero. Also at that region, y and z components of velocity equal to zero. Non-dimensional forms of the boundary condition can be written as:

at $\bar{z} = 0$ & $1 \geq \bar{x} \geq 0$ & $\frac{s}{2H} \geq \bar{y} \geq 0$

$$\frac{\partial \bar{u}}{\partial \bar{z}} = 0 \tag{3.38a}$$

$$\bar{v} = 0 \tag{3.38b}$$

$$\bar{w} = 0 \tag{3.38c}$$

$$\frac{\partial \theta}{\partial \bar{z}} = 0 \tag{3.38d}$$

3.3.6 Boundary Condition at z=W/2

This condition refers to lateral surface which is assumed to be insulated. At the lateral surface, all components of velocity are zero and since it is assumed to be insulated the slope of the temperature with respect to z axis also equals to zero. In the light of that information, non-dimensional form of the boundary conditions can be written as:

at $\bar{z} = \frac{W}{2H}$ & $1 \geq \bar{x} \geq 0$ & $\frac{s}{2H} \geq \bar{y} \geq 0$

$$\bar{u} = 0 \tag{3.39a}$$

$$\bar{v} = 0 \tag{3.39b}$$

$$\bar{w} = 0 \tag{3.39c}$$

$$\frac{\partial \theta}{\partial \bar{z}} = 0 \tag{3.39d}$$

3.4 PARAMETRIC SOLUTION OF THE PROBLEM

The preceding analyses lead to the conclusion that the solutions of the above governing equations for temperature depend on the following dimensionless groups which are $\bar{x}$, $\bar{y}$, $\bar{z}$, $Grx\Pr$, and $\frac{\dot{q}''H}{k(T_{w,\max} - T_\infty)}$.

The temperature distribution at the surface of the walls can be written as:

$$\theta = f\left(\bar{x}, \bar{y}, \bar{z}, Grx\Pr, \frac{\dot{q}''H}{k(T_{w,\max} - T_\infty)}\right) \tag{3.40}$$

In the most applications, it is not required to know all the details of the temperature field, but to know the quantity of the heat exchange between the plates and the air stream is necessary. This quantity can be expressed with the maximum temperature. The maximum temperature is referred as the temperature at the center of the walls at the exits and also it is assumed that temperature equals to the maximum wall temperature $\left(T_{w,\max}\right)$ for all points at the top of the plate. Therefore;

at $\bar{x} = 1$ ($x = H$), $\bar{y} = \frac{s}{2H}$ ($y = \frac{s}{2}$) and $\bar{z} = \frac{W}{2H}$ ($z = \frac{W}{2}$) $\Rightarrow T = T_{w,\max}$

The maximum dimensionless temperature is:

$$1 = f\left(1, \frac{s}{2H}, \frac{W}{2H}, Grx\Pr, \frac{\dot{q}''H}{k(T_{w,\max} - T_\infty)}\right) \tag{3.41}$$

From the equation (3.41), it can be written as:

$$\frac{\dot{q}''H}{k(T_{w,\max} - T_\infty)} = \varphi\left(\frac{W}{H}, \frac{s}{H}, Grx\Pr\right) \tag{3.42}$$

Then, that total heat exchange between the plates and the air stream for the whole electronic package can be calculated as:

$$\dot{Q}_{total} = \frac{\dot{q}''}{2} HW 2\frac{L}{s} \Rightarrow \dot{Q}_{total} = \dot{q}''HW\frac{L}{s} \tag{3.43}$$

From equation (3.42) and (3.43)

$$\frac{\dot{Q}_{total}H}{WLk(T_{w,\max} - T_\infty)} = \varphi\left(\frac{W}{H}, \frac{s}{H}, Grx\Pr\right)\frac{H}{s} \tag{3.44}$$

$$\Rightarrow \frac{\dot{Q}_{total}H}{WLk(T_{w,\max} - T_\infty)} = \phi\left(\frac{W}{H}, \frac{s}{H}, Grx\Pr\right) \tag{3.45}$$

for given $\frac{W}{H}$

$$\frac{\dot{Q}_{\max}H}{WLk(T_{w,\max} - T_\infty)} = \Lambda\left(\frac{s_{opt}}{H}, Grx\Pr\right) \tag{3.46}$$

CHAPTER 4

NUMERICAL SOLUTION AND RESULTS

4.1 NUMERICAL SOLUTION TECHNIQUE

In the numerical solution part of the current study, a commercial software FloEFD was used. FloEFD has been developed by the Mentor Graphics. Many companies including Aselsan A.Ş. use this computer program for the analysis of heat transfer and fluid flow problems in their designs because of its reliable results.

FloEFD software has a capability of solving both external and internal fluid flows, steady-state and time-dependent fluid flows, compressible gas and incompressible fluid flows, free, forced and mixed convection problems, fluid flow with boundary layers, including wall roughness effects, laminar and turbulent fluid flows, radiation heat transfer, flows of non-Newtonian liquids, flows of compressible liquids, real gases, two phase flows and so on [22].

FloEFD uses the Finite Volume Method (FVM) in order to solve the governing equations of the problems that indicated above. The unknowns in the discretized equations are found by using Semi-Implicit Method for Pressure-Linked Equations (SIMPLE) algorithm. In order to use the FVM in the solution of the problem, the computational domain should be divided into small control volumes. FloEFD uses structured Cartesian mesh; therefore, the rectangular parallelepipeds are the mesh cells in the computational domain [22].

4.1.1 Finite Volume Method

The finite volume method is the discretization of the integral form of the governing equations. The governing equations can be elliptic, parabolic, and hyperbolic type. In this thesis, governing equations are elliptic type. After the Boussinesq approximation, the momentum and energy equations for steady state problem can be written in general form as:

$$\rho u \frac{\partial \phi}{\partial x} + \rho v \frac{\partial \phi}{\partial y} + \rho w \frac{\partial \phi}{\partial z} = \Gamma\left(\frac{\partial^2 \phi}{\partial x^2} + \frac{\partial^2 \phi}{\partial y^2} + \frac{\partial^2 \phi}{\partial z^2}\right) + S_\phi \tag{4.1}$$

where ϕ is the transport variable and it corresponds to u, v, w, and T for x-momentum, y-momentum, z-momentum and energy equations respectively. Γ is the diffusion coefficient and it corresponds to μ for momentum equations and k/c for the energy equation. Finally, S_ϕ is the source function and it equals to $-\frac{\partial P}{\partial x} - \rho g$ for the x-momentum equation, $-\frac{\partial P}{\partial y}$ for the y-momentum equation, $-\frac{\partial P}{\partial z}$ for the z-momentum equation, and 0 for the energy equation.

In FloEFD, three-dimensional rectangular control volume is used throughout the discretization process of the general form of the governing equations. There is a general grid node mostly named with P inside the control volume. This point has 6 neighbors. These are generally called east, west, north, south, top, and bottom (see Fig. 4.1). It is not necessary to place the general grid node at the geometric center of the control volume. If it is placed at the geometric center of the control volume, then it is called cell-centered scheme. Estimating the flux values on the surfaces of the control volume and cell-centered scheme has an advantage at that point.

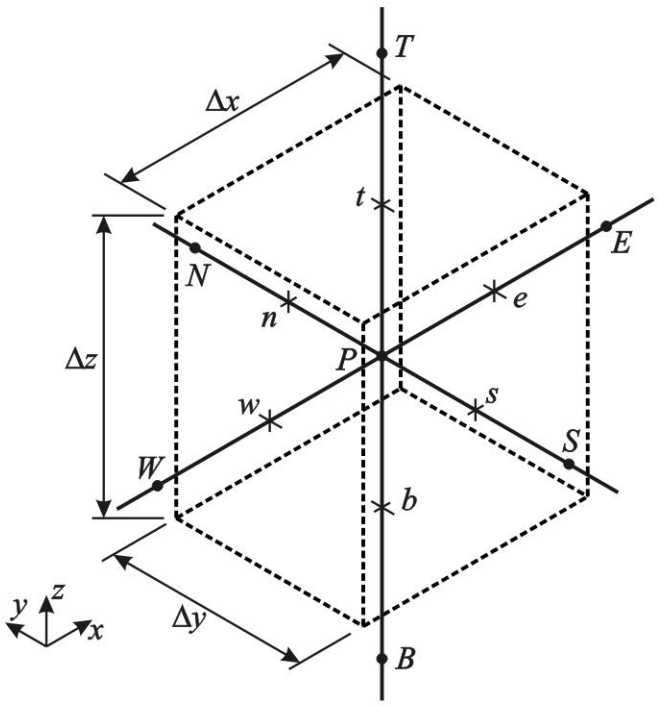

Fig. 4.1 3D Rectangular Control Volume

Different from the other computational fluid dynamic techniques such as finite difference and finite element methods, in the finite volume method, control volume integration of the general form of the governing equation is used. The results of the integration over the control volume that is specified above can be written as:

$$\begin{aligned}&\int_{CV}\rho u\frac{\partial\phi}{\partial x}dV+\int_{CV}\rho v\frac{\partial\phi}{\partial y}dV+\int_{CV}\rho w\frac{\partial\phi}{\partial z}dVt\\&=\int_{CV}\Gamma\frac{\partial^2\phi}{\partial x^2}dV+\int_{CV}\Gamma\frac{\partial^2\phi}{\partial y^2}dV+\int_{CV}\Gamma\frac{\partial^2\phi}{\partial z^2}dV+\int_{CV}S_\phi dV\end{aligned}\tag{4.2}$$

After the discretization procedure, the equation (4.1) becomes:

$$a_P\phi_P = a_E\phi_E + a_W\phi_W + a_N\phi_N + a_S\phi_S + a_T\phi_T + a_B\phi_B + \bar{S}\Delta V \qquad (4.3)$$

Equation (4.3) is the final form of the general transport equation after the discretization. Stabilization of the solution is guaranteed by the always positive coefficient rule. In order to achieve this rule, all coefficients in the equation (4.3) should be positive. Note that independently from the discretization scheme the coefficients from a_P to a_B are positive. Therefore, source term ($\bar{S}$) should be arranged according to always positive coefficient rule. The source term can be written as:

$$\bar{S} = S_U + S_P\phi_P \qquad (4.4)$$

In order to satisfy the always positive coefficient rule, it can be concluded from the equations (4.3) and (4.4):

$$S_U \geq 0 \qquad (4.5)$$

$$S_P \leq 0 \qquad (4.6)$$

4.1.2 The SIMPLE Method

The Semi-Implicit Method for Pressure-Linked Equations (SIMPLE) is used during the calculation of equations that mentioned above in FloEFD. This algorithm is a guess and correct type. The steps of the SIMPLE algorithm can be listed as [23]:

- Pressure field is estimated.
- Velocities in x, y, and z direction are found from the momentum equations by using estimated pressure field.
- Pressure correction equation is solved; and correct values of the pressure and the velocity components are found.

- The value of temperature is found by using correct pressure, velocity components, and energy equation.
- Found temperature does not converge, then a new estimation is done and steps are repeated.
- If it converges, then procedure finishes.

4.1.3 Definition of Initial Properties

At the beginning of the project, FloEFD needs some properties to use in the solution of the numerical problem. Throughout the analyses, 24°C air is used as an ambient (T_∞= 24°C).

In the mathematical model, the effect of radiation is neglected. Therefore, throughout the numerical solution, the equations related to the radiation are not calculated. In the modeling of the problem, flow is assumed as incompressible; hence, density is constant in the calculations.

4.1.4 Setting the Boundary Conditions at the Inlet and Outlet $(\bar{x}=0)$ $(\bar{x}=1)$

In the model of the channel, there are no obstacles at the inlet and the outlet. It is an open channel flow. Therefore, there is no information about the flow distribution inside the channel. Only pressures are known. At these circumstances, the constant pressure boundary condition is used for both the inlet and the outlet. In order to achieve the inlet and the outlet boundary condition, the pressure correction is taken as zero. A convenient way to adjust the pressure correction to a zero is to arrange the source function as follows:

$$S_U = 0 \tag{4.7}$$

$$S_P = -10^{30} \tag{4.8}$$

4.1.5 Setting the Boundary Condition at y=s/2

This boundary condition refers to surface of the plates where the constant heat flux is applied to walls. The surface of the plates is assumed to be ideal in the mathematical model; therefore, velocities are 0 at the wall surface. For this boundary condition source, equations are defined as:

$$S_U = \frac{1}{\Delta V}\frac{\dot{q}''\Delta y}{c_p} \tag{4.9}$$

$$S_P = -\frac{\mu}{\Delta y_P} A_{cell} \tag{4.10}$$

Setting the source equations in equations (4.7) and (4.8) provides both the boundary condition and always positive coefficient rule.

4.1.6 Setting the Boundary Condition at y=0

At y= s/2, constant heat flux condition is defined. Also this boundary condition is valid for y= -s/2. Therefore, the computational domain is symmetric along y-direction. Because of that definition, at y= 0, a symmetry plane occurs and there are no flow and no scalar flux across the symmetry plane. In that case, the control volumes in both sides of the symmetry plane are identical. In the numerical solution, that type of boundary condition can be defined as follows:

$$\phi_{1,J} = \phi_{2,J} \tag{4.11}$$

Also, the coefficient of the discretized pressure correction equation is set to zero for the solution of symmetric boundary condition. Therefore, using the above definition, condition at y= 0 (equations (3.36a-3.36d)) is satisfied for the problem.

4.1.7 Setting the Boundary Condition at z= W/2

Velocities equal to zero and the slope of the temperature with respect to z axis also equals to zero since the lateral edges are assumed to be closed and insulated. This boundary condition (equations (3.43a-3.43d)) is satisfied by the arranging the source equations as follows:

$$S_U = 0 \tag{4.12}$$

$$S_P = 0 \tag{4.13}$$

4.1.8 Setting the Boundary Condition at z= 0

In Chapter 3, the lateral edges of the computational domain are defined as insulated. Therefore, both z= W/2 and z= -W/2 are insulated. This makes the computational domain symmetric along z-direction. Because of that definition, at z= 0, a symmetry plane occurs as same as y= 0 plane in Section 4.1.6. Therefore, the same condition in section 4.1.6, which is no flow and no scalar flux across the symmetry plane, is valid for this case. In order to satisfy the boundary condition, the coefficient of the discretized pressure correction equation is set to zero. The definition of the symmetry boundary condition is basically:

$$\phi_{1,J} = \phi_{2,J} \tag{4.14}$$

4.1.9 Meshing the Computational Domain

A proper meshing of the computational domain is the essential for the accurate result of the numerical solution. In FloEFD, meshing is easier than the most of the other analysis software. Simply, in FloEFD level of mesh intensity and the level of mesh refinement are selected and the rest of the work is done by software. In the current thesis, dimensions of the cells are 0.5 mm x 0.5 mm x 0.5 mm near the walls. On the other hand, at the middle section of the computational domain,

dimensions of the cell are between 1 mm x 1 mm x 1 mm and 2 mm x 2 mm 2 mm depending on the spacing between two plates. Approximately, number of cell that used in the solution of the computational domain alters between 1000000 and 2000000 depending on the dimensions of the computational domain.

4.2 ANALYSIS PROCEDURE

Natural convection cooling in the array of parallel and vertical plates at constant heat flux is investigated in the thesis as modeled in Chapter 3. Width of the heat generating boards is constant and equals to 150 mm for all analyses. Height of the plates, on the other hand, changes from 300 mm to 10 mm in order to investigate the aspect ratio effects on optimum spacing between the array of parallel and vertical heat generating boards under natural convection. Ambient temperature in the analyses is constant and equals to the 24°C. Constant heat fluxes that conclude 20°C to 50°C temperature difference between the ambient and the maximum temperature of the wall are defined to the heat generating boards.

8 different heights are calculated which are 300 mm, 250 mm, 200 mm, 150 mm, 100 mm, 30 mm, 15 mm, and 10 mm. In other words, aspect ratio of the plates changes between 0.5 and 15. 300 mm and 10 mm heights are calculated in order to see the situation in the extreme points. The other 6 heights are also calculated because printed circuit boards in these dimensions are used in defense industry commonly. Therefore, finding optimum spacing for these aspect ratios is helpful for engineers that working on thermal management of devices including vertical and parallel printed circuit boards in it.

In the first configuration, height (300 mm) of the plates is very long with respect to its width (150 mm). Aspect ratio equals to 0.5 in this configuration. Also, in this dimension, for different spacing values which are between changing 4 mm and 50 mm are calculated. For each spacing, 20°C to 50°C temperature increase is found by applying proper heat transfer rate.

Furthermore, 4 analyses are conducted for plates in which heights change between 250 mm and 100 mm. In other words, aspect ratio changes between 0.6 and 1.5. Spacing between plates varies from 4 mm to 50 mm. Again as in the first analysis, different heat dissipation rates that resulted in 20°C to 50°C temperature difference in plates are applied.

In the last three analyses, plate heights are 30 mm, 15 mm, and 10 mm and, as in the all analyses, width of the plate is 150 mm. Note that, this is an extreme point in which aspect ratio approaches to infinity. Since the plates are shorter than the plates in other configurations, optimum spacing is thought to be in smaller value than the other analyses. Therefore, in this case, different spacing between 2 mm and 6.5 mm are calculated. Constant heat flux case is also applied to this case. Approximately 15- 18 different heat fluxes that resulted in 20°C to 50°C temperature difference in plates are applied to two vertical and parallel plates for all spacing.

To conclude, during the analyses, 65 different vertical and parallel plate configurations are analyzed under natural convection cooling. Also, for all of the 65 configurations, various rate of heat dissipation are applied. Totally, more than 1100 analyses are conducted for the current thesis.

4.3 RESULTS OF THE NUMERICAL SOLUTION

Numerical analyses are performed for the plate heights of 10 mm to 300 mm. Plate spacing are varied from 2 mm to 50 mm depending on the height of the plate. Heat flux rate from the heat generating boards are varied between 20 W/m^2 and 900 W/m^2. In this section of the thesis, the results of the numerical solution are presented. The graphs which show the results of the numerical solution represent the change of dimensionless heat transfer rate from the plates to ambient $\left(\frac{\dot{q}''H}{k(T_{w,\max}-T_{\infty})}\right)$ with the ratio of the spacing to the plate height $\frac{s}{H}$ for two plates for some constant $Grx\Pr$ dimensionless group (Fig. 4.2– 4.9).

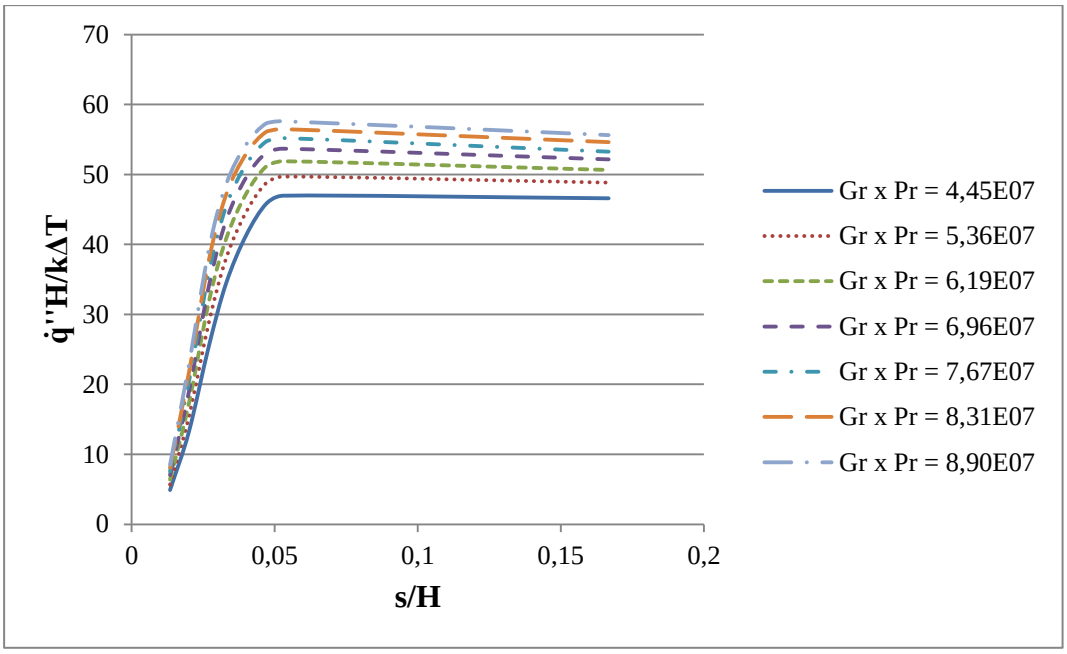

Fig. 4.2 Variation of Dimensionless Heat Transfer Rate $\left[\dot{q}''H/k(T_{w,\max}-T_{\infty})\right]$ with the Ratio of the Spacing to the Plate Height (s/H) for W/H = 0.5

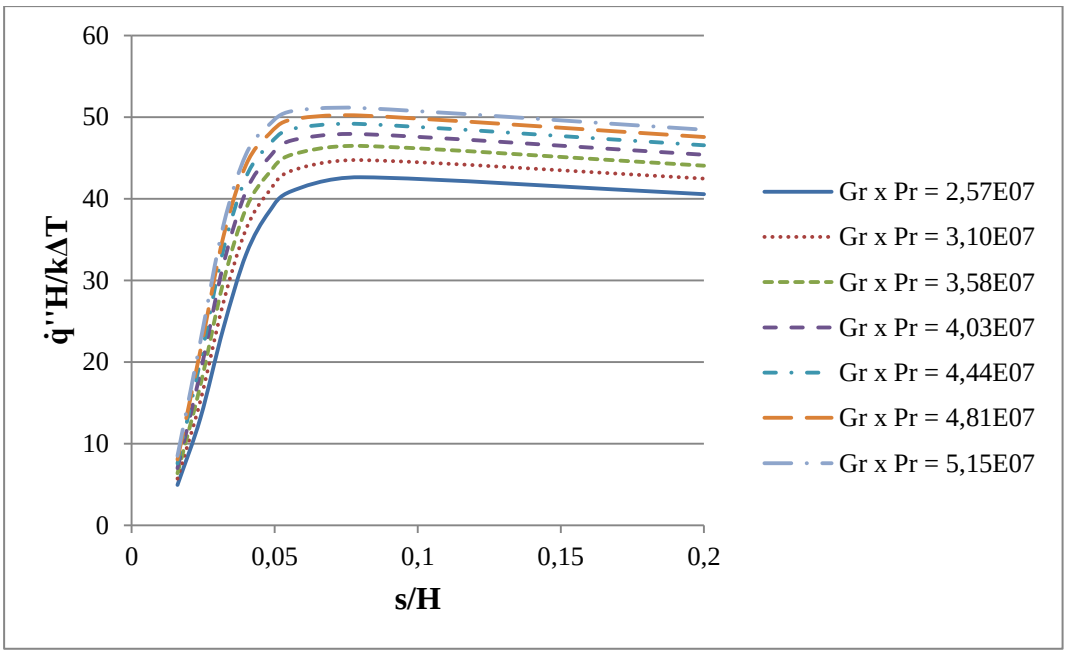

Fig. 4.3 Variation of Dimensionless Heat Transfer Rate $\left[\dot{q}''H/k(T_{w,\max}-T_{\infty})\right]$ with the Ratio of the Spacing to the Plate Height (s/H) for W/H = 0.6

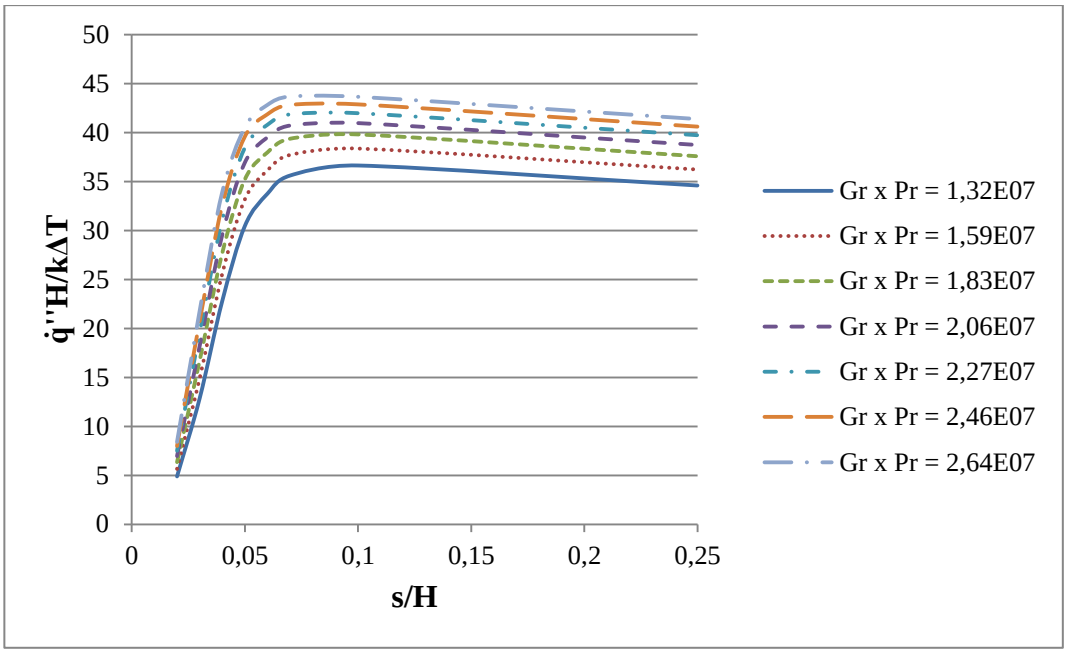

Fig. 4.4 Variation of Dimensionless Heat Transfer Rate $\left[\dot{q}''H/k(T_{w,\max}-T_{\infty})\right]$ with the Ratio of the Spacing to the Plate Height (s/H) for W/H = 0.75

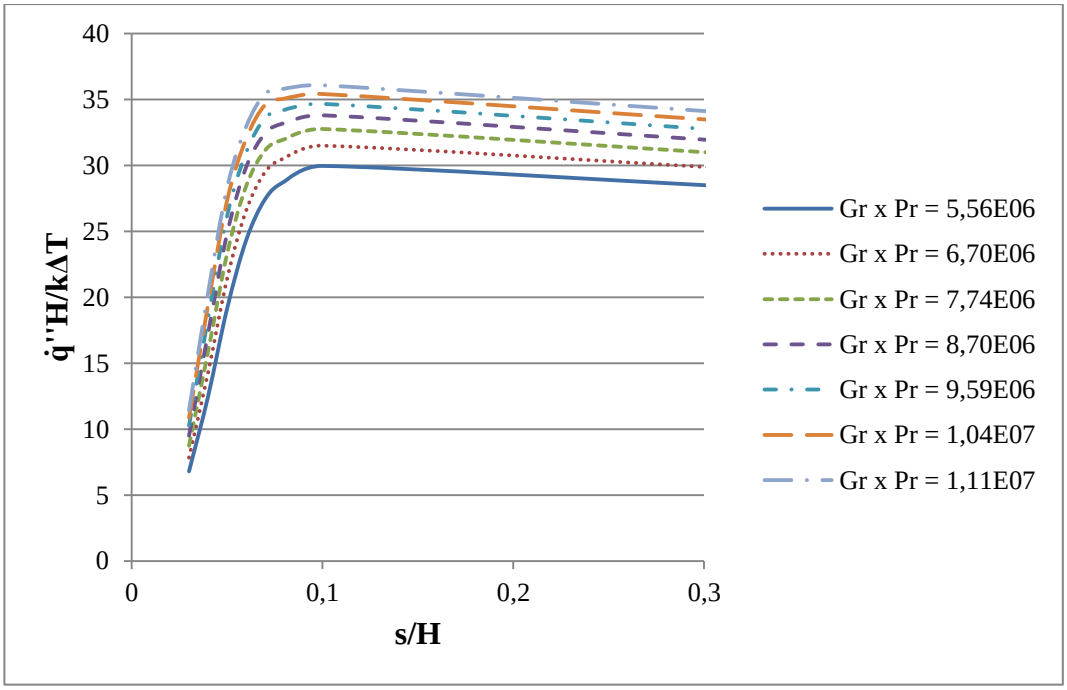

Fig. 4.5 Variation of Dimensionless Heat Transfer Rate $\left[\dot{q}''H/k(T_{w,\max}-T_{\infty})\right]$ with the Ratio of the Spacing to the Plate Height (s/H) for W/H = 1

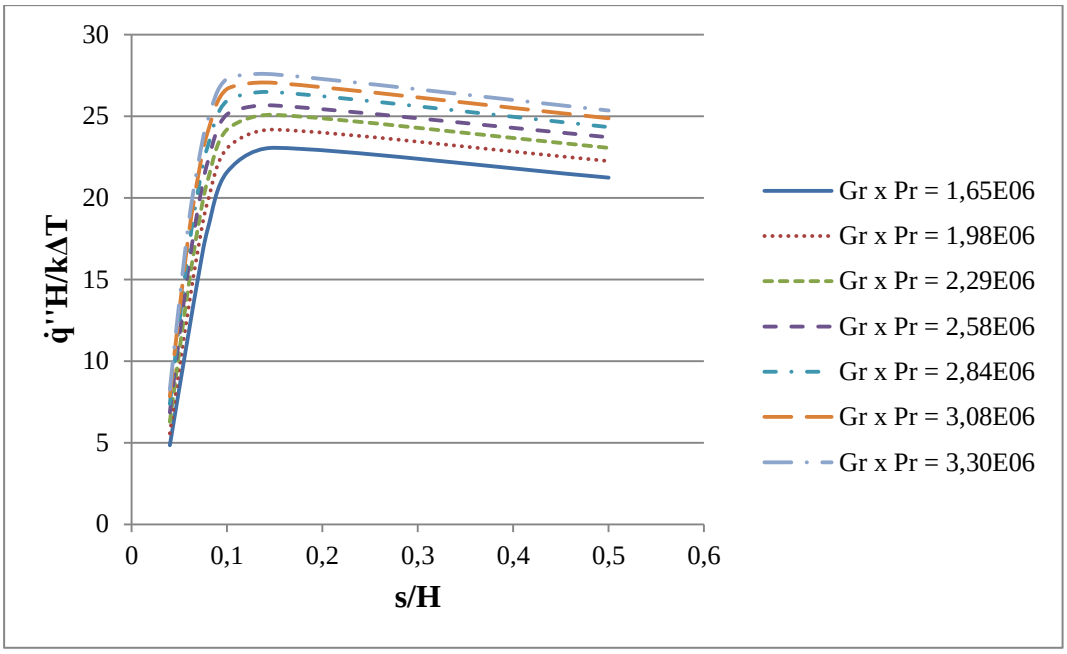

Fig. 4.6 Variation of Dimensionless Heat Transfer Rate $\left[\dot{q}''H/k(T_{w,\max}-T_{\infty})\right]$ with the Ratio of the Spacing to the Plate Height (s/H) for W/H = 1.5

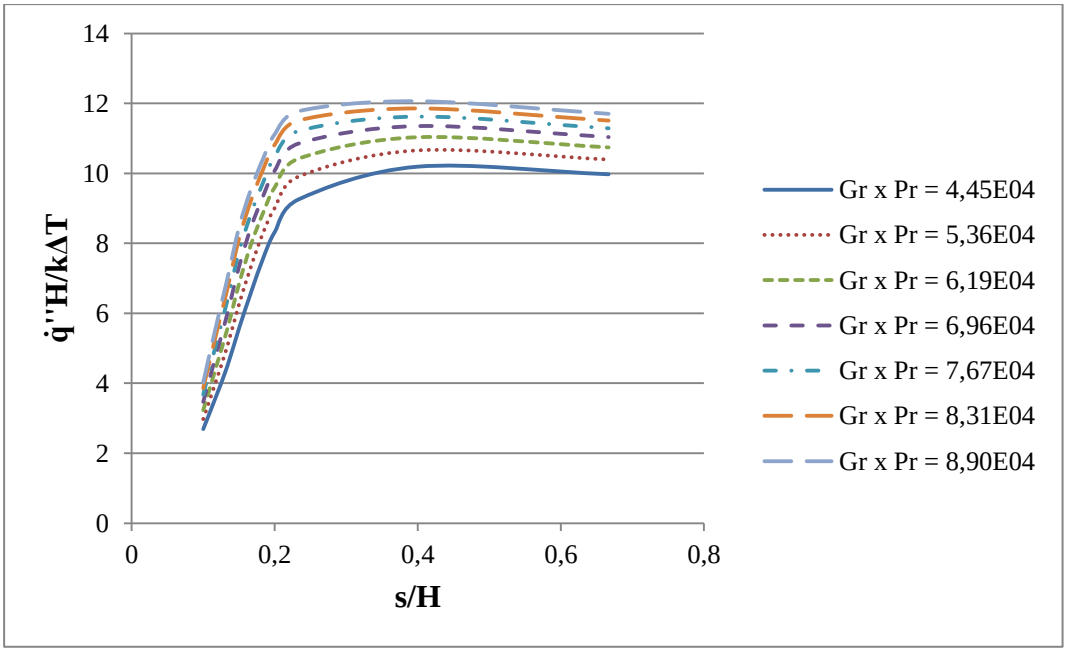

Fig. 4.7 Variation of Dimensionless Heat Transfer Rate $\left[\dot{q}''H/k(T_{w,\max}-T_{\infty})\right]$ with the Ratio of the Spacing to the Plate Height (s/H) for W/H = 5

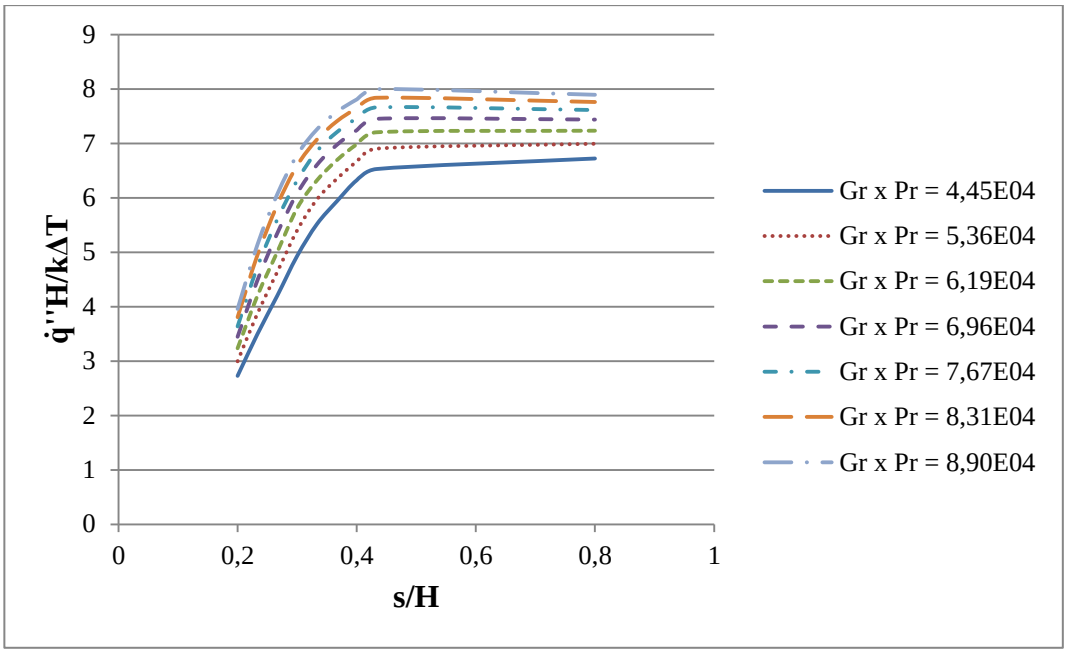

Fig. 4.8 Variation of Dimensionless Heat Transfer Rate $\left[\dot{q}''H/k(T_{w,\max}-T_{\infty})\right]$ with the Ratio of the Spacing to the Plate Height (s/H) for W/H = 10

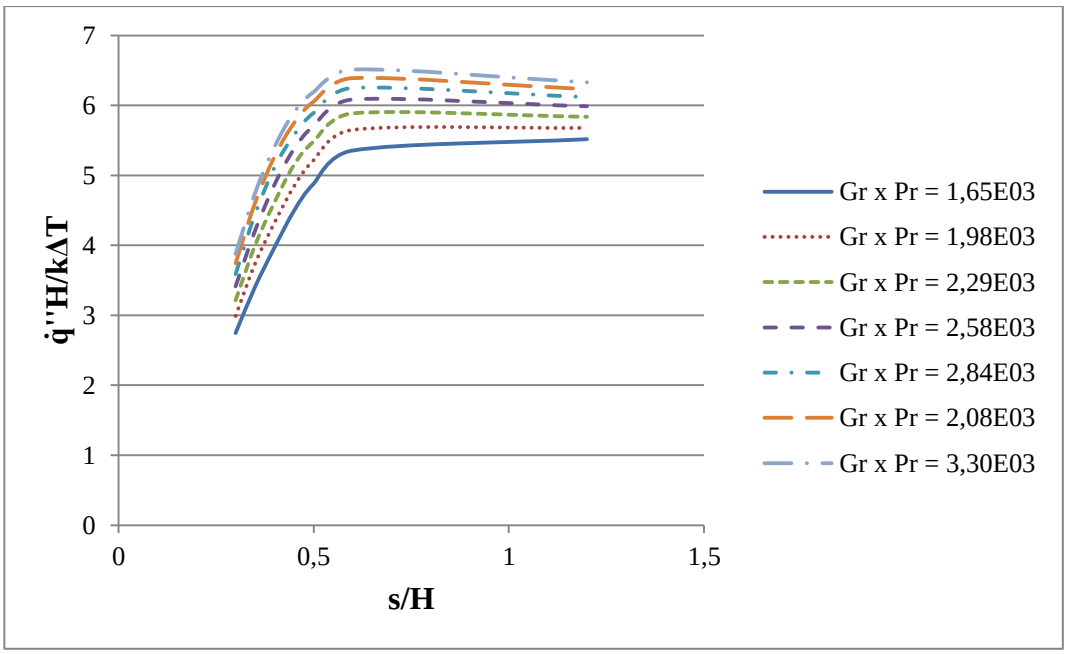

Fig. 4.9 Variation of Dimensionless Heat Transfer Rate $\left[\dot{q}''H/k(T_{w,\max}-T_{\infty})\right]$ with the Ratio of the Spacing to the Plate Height (s/H) for W/H = 15

CHAPTER 5

EXPERIMENTAL STUDY

Solving an engineering problem by using a computer program makes the life easier for engineers. However, modeling the real life on computer program does not give the real results always. The objective of this experimental work is to verify the present numerical simulations. In this chapter, first the experimental setup is described. Secondly, the results of the experiments are introduced. Finally, numerical code for certain case is compared by the experimental result.

5.1 EXPERIMENTAL SETUP

Experimental setup consists of a casing of the fixed volume with supporting frame and various instruments. Casing is made of delrin which is easily machinable and thermally non-conductor material. There are 1.1 mm slots in the side walls of the casing; therefore, machinability of the delrin is provided easy manufacture. Thermal conductivity of delrin which provides the minimum heat loss from the edges of plates to the casing is 0.4 W/mK [24]. The length of the casing is 60 mm, the height of the casing is 200 mm, and the width of the casing is 150 mm. Wall thickness is 10 mm. 13 slots are machined to the side walls of the casing in order to place the plates. Fig. 5.1 shows the casing that is used in the experiments.

Copper plates are used as a heat generating boards in the experiments. Plates are heated uniformly in order to satisfy uniform heat flux condition that is the reason of the using copper plates as a heat generating boards is its high thermal conductivity (k = 400 W/mK) [25]. However, electrical resistance of the copper

plate is too low to heat by DC power supply. Therefore, heating spirals in which resistance is 7.4 Ω/m are used in order to heat the plates at constant heat flux. Heating spirals are wrapped around the copper plates by using non-conductor tape at intervals of 3 cm. In order to wrap a plate, 900 mm heating spirals are used. Hence, resistance of the plates becomes 6.7 Ω.

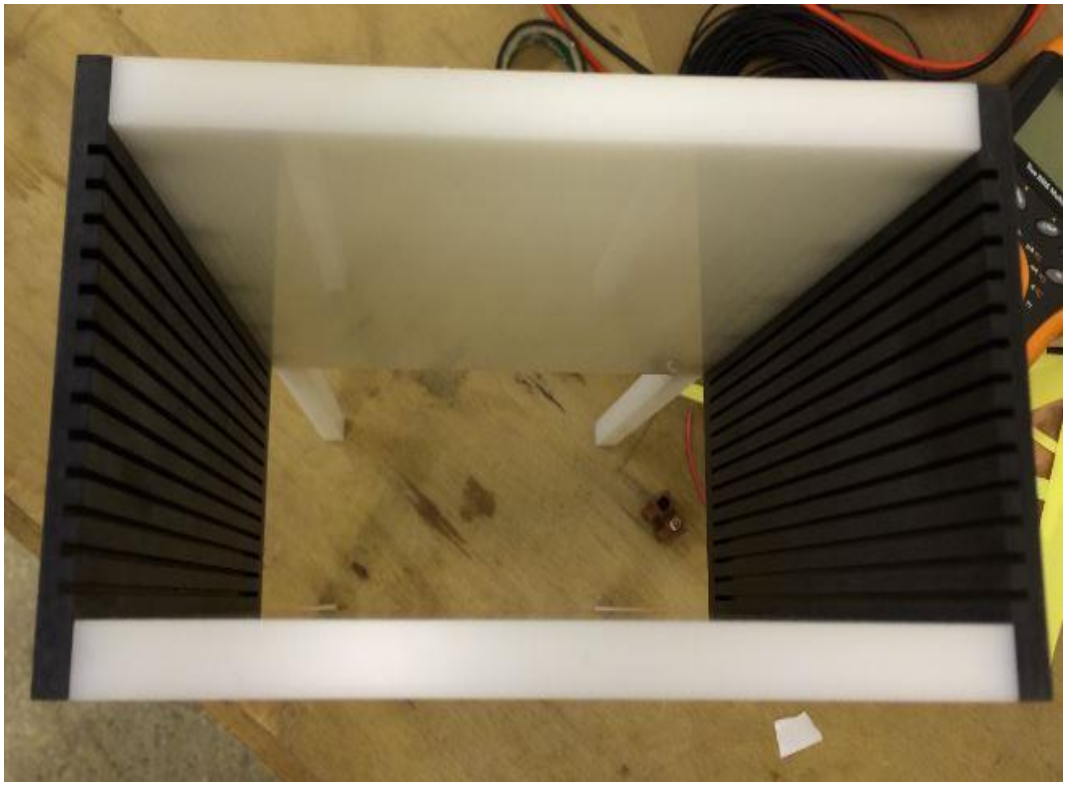

Fig. 5.1 Casing

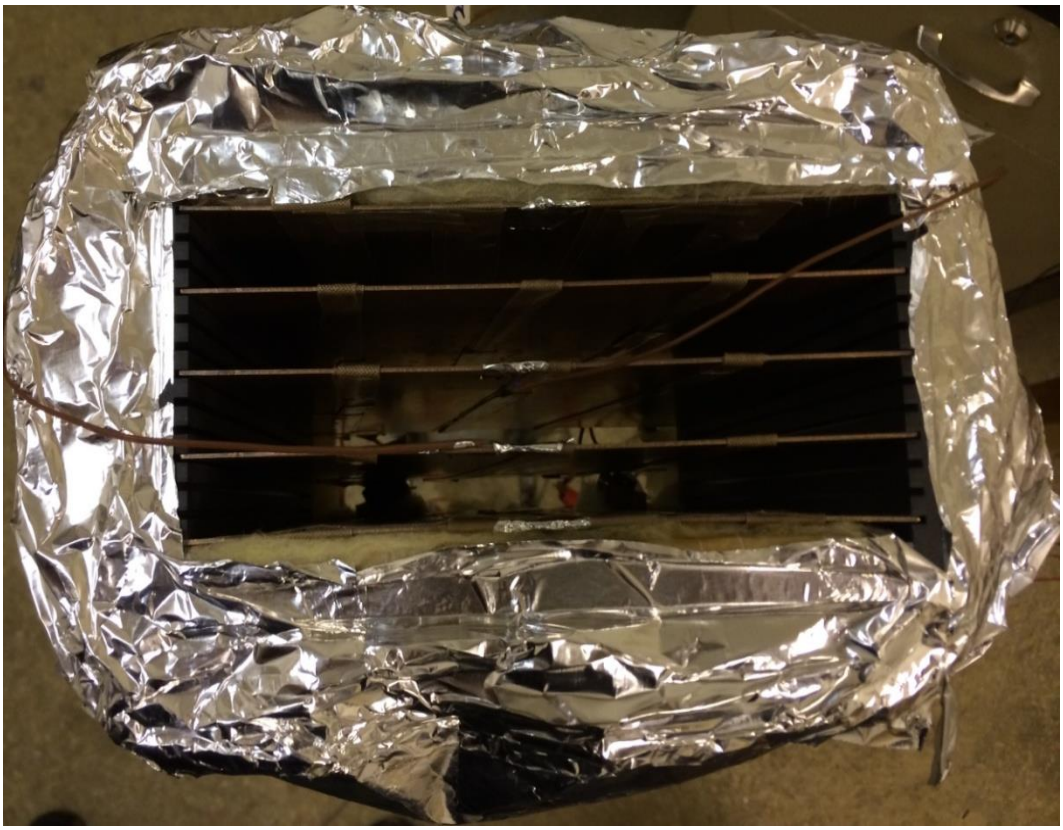

Fig 5.2 Casing After Insulation

The thermal conductivity of delrin is low; however, heat loss from the outer edges of the casing is inevitable. Therefore, insulation is used all around the casing. Fiberglass is chosen as an insulation material for the experimental set up. The thermal conductivity of the fiberglass is very low (k = 0.04W/mK). All the four surfaces of the casing are surrounded by fiberglass along the whole length of the walls. The thickness of the fiberglass that used in the sides of the casing is 30 mm. Fiberglass is placed between the casing and the rear sides of the first and the last plates. Because, when mathematical model is extended to an array, only one side of the first and the last plates are exposed to uniform heat flux (see Fig. 5.2).

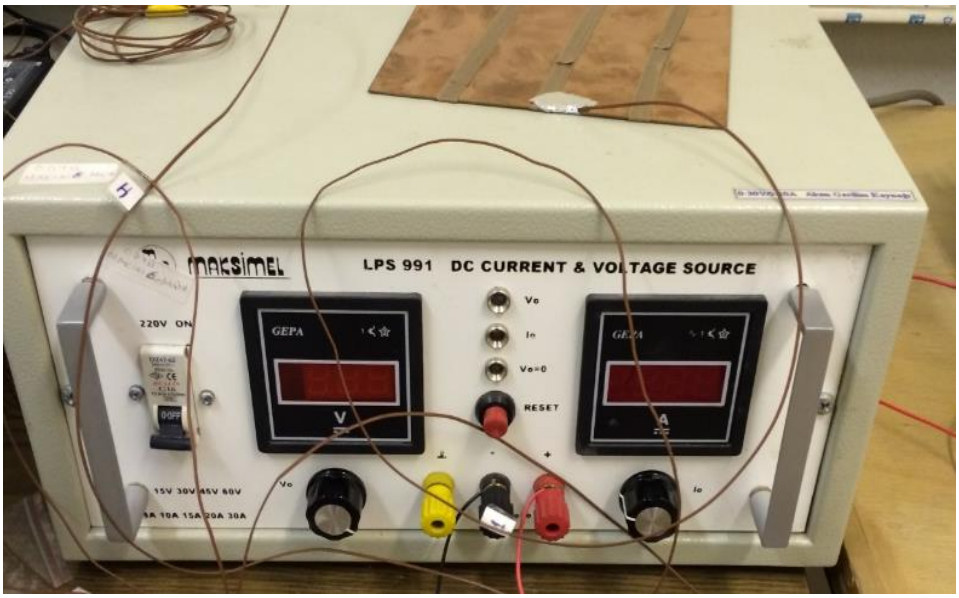

Fig. 5.3 DC Power Supply #1

In the mathematical model, boundary condition at the heat generating boards is defined as uniform heat flux. In order to satisfy this condition, heating spirals are wrapped around the plates. Then, these heating coils are heated by DC power supply.

Two power supplies are used in order to control plates separately. One of those two power supplies is connected to the first and the last plates since only one surface of these plates is wrapped by heating coils; therefore, the resistance on those plates is different from the plates that are placed to inner part of the package. The other DC power supply is used to supply electrical energy to the plates which are placed between the first and the last plates. The number of plates that connected to the second power supply changes by changing number of plates in the fixed volume. Fig. 5.3 and Fig. 5.4 show the power supplies.

Fig. 5.4 DC Power Supply #2

Preparing experimental setup properly is an important issue to obtain reliable results. Also, reading the correct values of the temperature from the surface of the plate is as important as preparing the proper experimental setup. Thermocouples are used in order to measure temperature values from the surface of the plates correctly. Thermocouples are connected to the data acquisition system (see Fig. 5.5); and then, thermocouples are installed at the middle top of the plates since maximum surface temperature occurs at that point. The thermocouples that are used in the experimental study are T-type. By using T-type thermocouples, one can read temperatures between -200°C and 350°C. If the temperature is between -60°C and 100°C, then the error is 1°C. [26] Data from the plates are saved at intervals of 1 minute along the 24 hours until the system is reached to the steady-state.

The whole setup is built up through inserting all of its parts (i.e. thermocouples, and cables from the power supplies) to the plates in the casing. This whole setup is placed to the 80 cm above from the ground by using supporting frame in order to provide proper air flow from the bottom of the system (see Fig. 5.6).

Fig. 5.5 Data Acquisition Unit

Fig. 5.6 Experimental Setup

5.2 EXPERIMENTAL PROCEDURE

Experiments are conducted in order to verify the result of the theoretical solution. In the experiments, only one aspect ratio which is W/H= 0.75 (H= 200 mm & W= 150 mm) is investigated for 4 different configurations. In the first configuration, 4 plates are inserted to the system with equal distances. Therefore, spacing between

plates equals to 20 mm. Then, by using power supply, uniform heat flux from the plates is provided. 7 different heat inputs from 12 W to 56 W are tested for this configuration; and maximum wall temperatures occurs at the middle top of the plate are noted.

In the second configuration, number of plates in the casing is increased to 5. Spacing between the plates becomes 15 mm at this settlement. For this configuration, 9 different heat inputs between 16 W and 80 W are applied to the system.

Then, spacing between plates is decreased to 10 mm by installing 7 plates to the assembly. For this configuration, 8 different heat inputs between 24 W and 108 W are applied to the system. Again maximum temperatures of the plates are noted for each heat input value.

Lastly, all slots of the casing are completed. 13 plates are inserted to the system. Therefore, spacing between plates becomes 5 mm in this configuration. 9 different heat inputs from 7.2 W to 74.4 W are tested for this configuration; and as in all of the previous steps, maximum wall temperatures at the middle top of the plate are noted.

5.3 EXPERIMENTAL RESULTS

In the previous section, configurations that are conducted in experiment are explained. Basically, 4 different spacing values which are 20 mm, 15 mm, 10 mm, and 5 mm are investigated. Therefore, during the experiments number of plates in the fixed volume changes between 4 and 13. In this part of the current thesis, results of those experiments are introduced. Total heat transfer rate from the fixed volume, maximum temperature that occurs on the surface of the plates and the ambient temperature is tabulated as shown in the Table 5.1.

Table 5.1 Experimental Results for W/H = 0.75

s/H= 0.1			s/H= 0.075			s/H= 0.05			s/H= 0.025		
$\dot{Q}_{total}$ (W)	$T_{w,max}$ (°C)	T_{∞} (°C)	$\dot{Q}_{total}$ (W)	$T_{w,max}$ (°C)	T_{∞} (°C)	$\dot{Q}_{total}$ (W)	$T_{w,max}$ (°C)	T_{∞} (°C)	$\dot{Q}_{total}$ (W)	$T_{w,max}$ (°C)	T_{∞} (°C)
12	28	14	16	34	19	24	40,5	22	7,2	34	20
18	33	14	24	34	14	36	44,3	20	15,6	41	20
25,5	40	16	32	39	15	48	48	19	24	49	21
33	44	15	40	44	16	60	56,5	22	32,4	54	20
40,5	52	17	48	49	17	72	63,5	24	40,8	60	21
48	57	17	56	53	16	84	67	23	49,2	64	21
55,5	60	15	64	58	17	96	68	19	57,6	68	21
			72	63	18	108	72	19	66	71	20
			80	66	17				74,4	75	20

5.4 COMPARISON OF RESULTS OF NUMERICAL SOLUTION AND EXPERIMENTAL STUDY

The importance of verifying the results of analyses with experiments has been explained at the beginning of this section. In order to prove the validity of numerical solution method, the dimensionless maximum temperature obtained in experimental results are compared with the available numerical calculations. The dimensionless temperature difference has been previously defined in equation (3.41). The dimensionless temperature difference was:

$$\frac{T-T_\infty}{T_{w,\max}-T_\infty}=\theta=1=f\left(1,\frac{s}{2H},\frac{W}{2H},Grx\,\mathrm{Pr},\frac{\dot{q}''H}{k(T_{w,\max}-T_\infty)}\right) \tag{5.1}$$

From the equation (5.1) it can be written as:

$$\frac{\dot{q}''H}{k(T_{w,\max}-T_\infty)}=\varphi\left(\frac{W}{H},\frac{s}{H},Grx\,\mathrm{Pr}\right) \tag{5.2}$$

For constant s/H and W/H equation (5.2) becomes:

$$1=\Psi\left(Grx\,\mathrm{Pr},\frac{\dot{q}''H}{k(T_{w,\max}-T_\infty)}\right) \tag{5.3}$$

From the equation (5.3):

$$Grx\,\mathrm{Pr}\approx\frac{\dot{q}''H}{k(T_{w,\max}-T_\infty)} \tag{5.4}$$

As a conclusion of equation (5.3) variation of dimensionless heat transfer rate $\left(\dot{q}''H/k\Delta T\right)$ with dimensionless group $\left(Grx\,\mathrm{Pr}\right)$ is plotted. Note that graphs are in logarithmic scale is used for all four cases when comparing results.

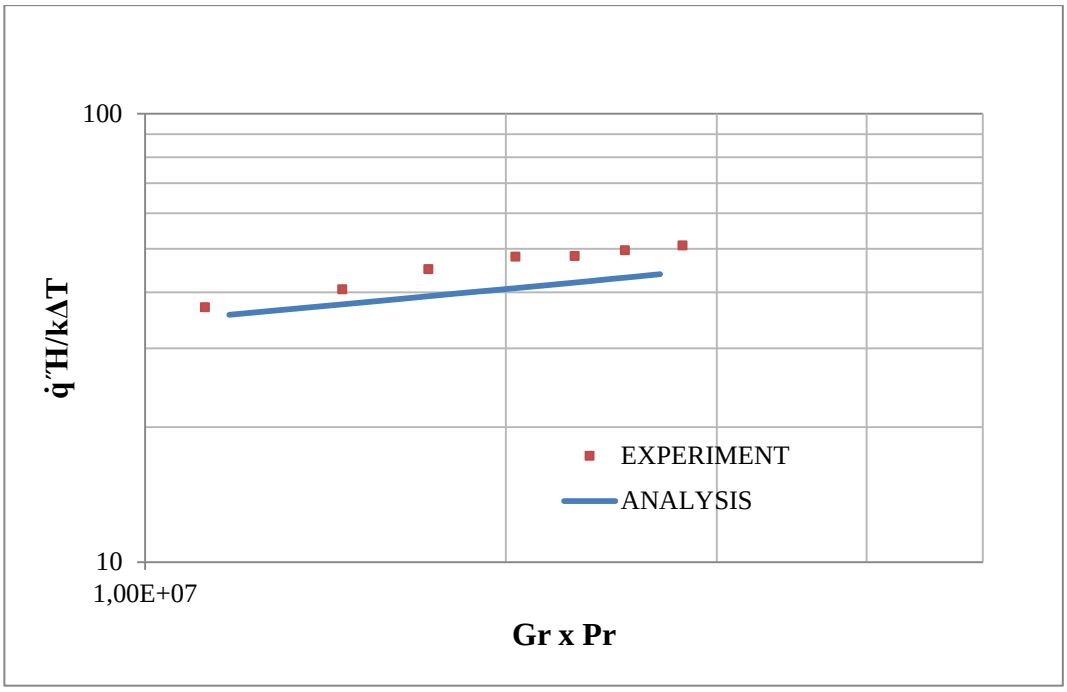

Fig. 5.7 Comparison of Results of Experiments and Analyses

(s/H = 0.1 & W/H= 0.75)

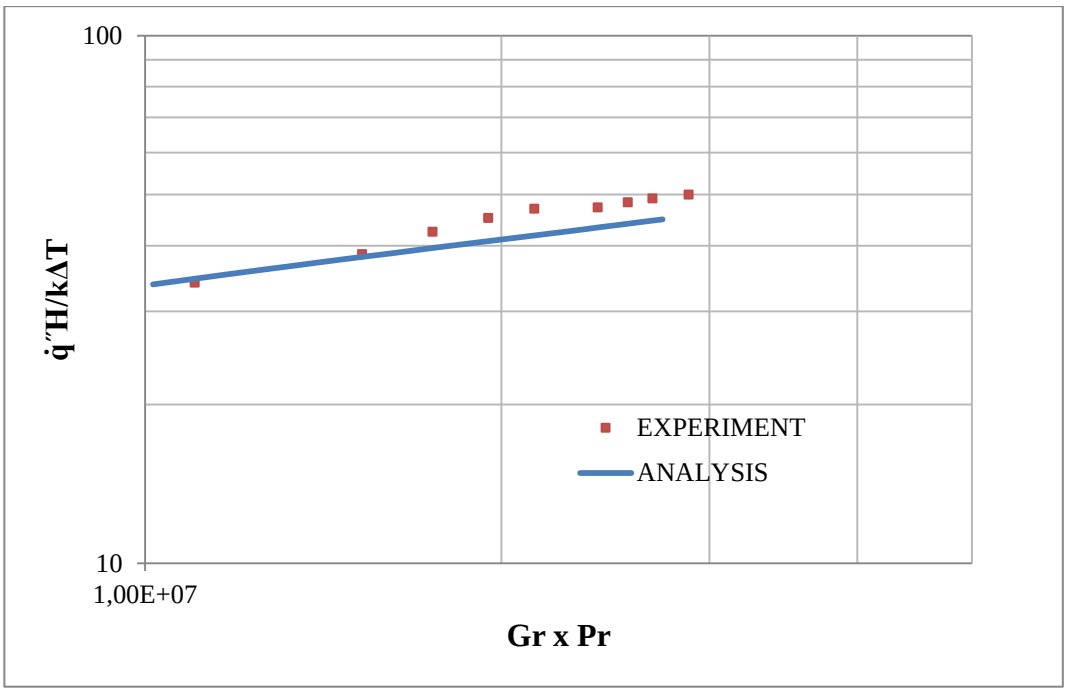

Fig. 5.8 Comparison of Results of Experiments and Analyses

(s/H = 0.075 & W/H= 0.75)

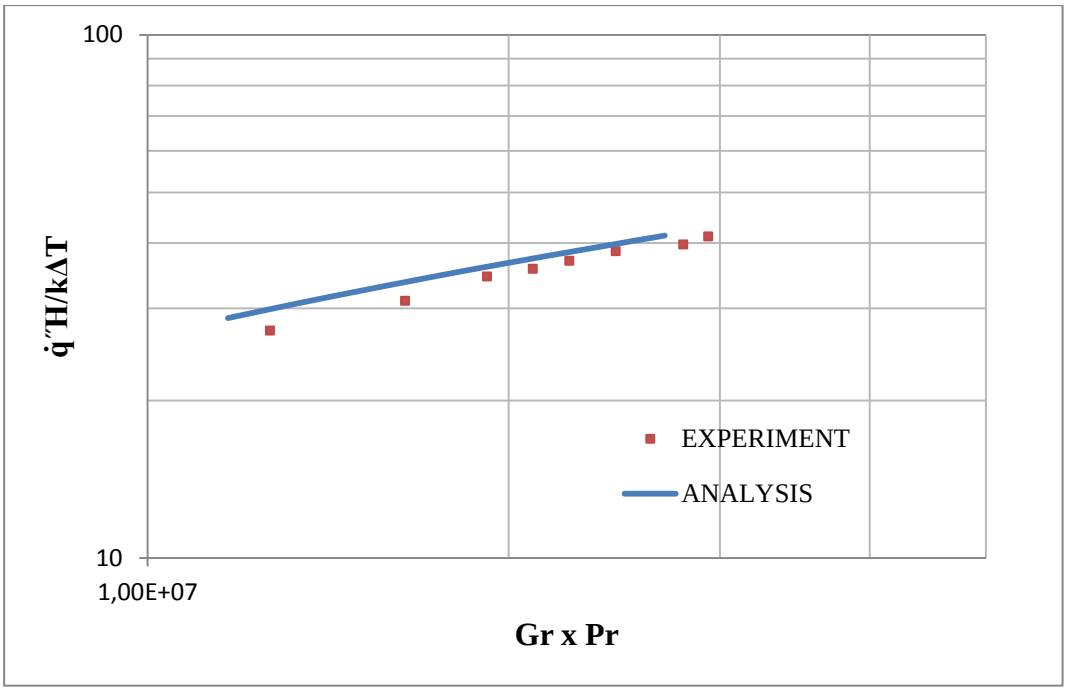

Fig. 5.9 Comparison of Results of Experiments and Analyses

(s/H = 0.05 & W/H= 0.75)

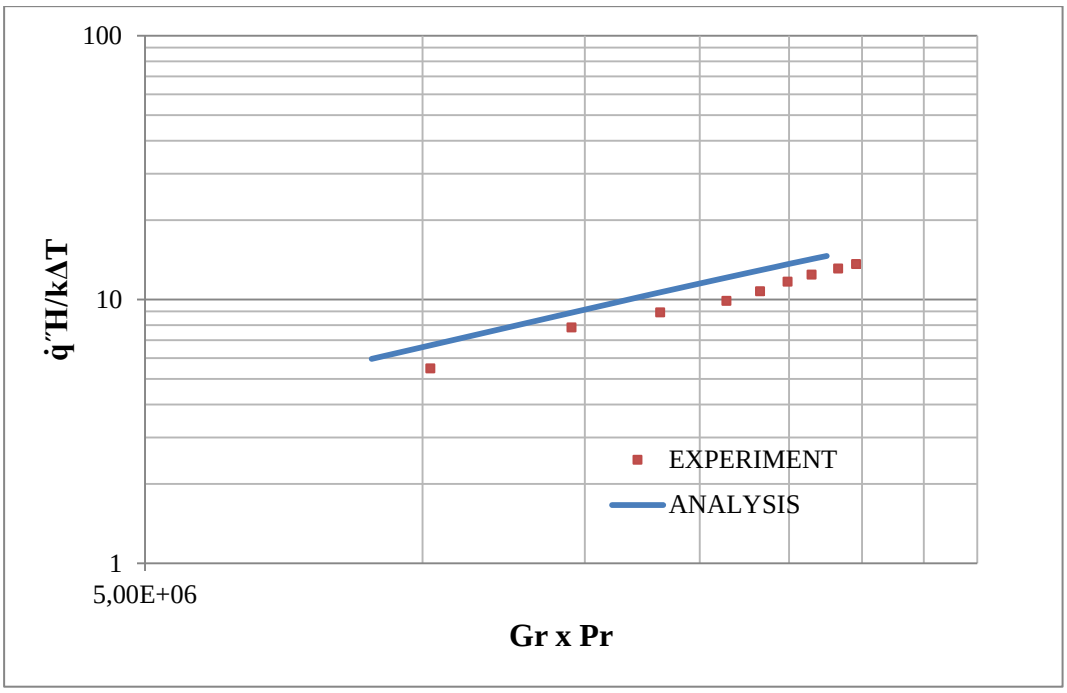

Fig. 5.10 Comparison of Results of Experiments and Analyses

(s/H = 0.025 & W/H= 0.75)

It is obvious in the figures (Fig. 5.7- 5.8- 5.9- 5.10), results of analyses and experiments are close to each other. The trend of the increase of the dimensionless heat transfer rate $\dot{q}''H/k\Delta T$ is same for both analysis and experiments. However, there is a difference between the results of numerical and experimental studies. In order to find the deviation between the results of numerical study and the experimental study equation (5.5) is used.

$$\text{Relative Error} = \left| \frac{\text{Experimental value - Numerical value}}{\text{Numerical value}} \right| \times 100 \qquad (5.5)$$

By using equation (5.5) the maximum relative error for s/H= 0.1 is 17%. For the second configuration (s/H= 0.075), the maximum relative error is 12%. The maximum relative error for the s/H= 0.05 is 10%. Finally, when the s/H= 0.025, the maximum relative error becomes 19%. As it can be seen from those results the maximum relative error throughout the study equals to 19% and it occurs when the s/H= 0.025. Reasons of those errors are explained in Chapter 7 in detail.

CHAPTER 6

OPTIMIZATION

6.1 OPTIMIZATION PROCEDURE

Up to this point, convective heat transfer characteristics between two vertical and parallel plates are discussed. The design of electronic components requires mounting as much circuits as possible in a given space. Therefore, in the electronic packages arrays of heat generating printed circuit boards (PCBs) are placed in a fixed volume as close as possible. In this part of the study, plates are stacked in a fixed volume and process that mentioned in Chapter 3 is applied to the package (see Fig. 3.2) and heat flux is obtained as follows:

$$\frac{\dot{q}''H}{k(T_{w,\max}-T_{\infty})}=\varphi\left(\frac{W}{H},\frac{s}{2H},Grx\Pr\right) \tag{6.1}$$

Since there is L/s plate in a fixed volume $\dot{Q}_{total}$ is found as:

$$\dot{Q}_{total}=\frac{\dot{q}''}{2}HW2\frac{L}{s}\Rightarrow\dot{Q}_{total}=\dot{q}''HW\frac{L}{s} \tag{6.2}$$

If the equation (6.1) and (6.2) combined the equation (6.3) is found.

$$\frac{\dot{Q}_{total}H}{WLk(T_{w,\max}-T_{\infty})}=\varphi\left(\frac{W}{H},\frac{s}{2H},Grx\Pr\right)\frac{H}{s} \tag{6.3}$$

$$\Rightarrow \frac{\dot{Q}_{total} H}{WLk(T_{w,\max} - T_{\infty})} = \phi\left(\frac{W}{H}, \frac{s}{H}, Grx\Pr\right) \tag{6.4}$$

In the optimization procedure; first, the change of dimensionless total heat transfer rate $\left(\dot{Q}_{total} H / WLk(T_{w,\max} - T_{\infty})\right)$ with respect to ratio of spacing between plates to the height of the plate (s/H) is plotted for different aspect ratios (W/H) for constant dimensionless groups (Gr x Pr). Secondly, an optimum s/H value where the dimensionless total heat transfer rate is maximum value is found. Then, the ratio of the optimum spacing between plates to the height of the plate for constant Gr x Pr numbers is tabulated and change of between them is plotted. An optimum spacing in the form of equation (6.6) is established between s_{opt}/H and Gr x Pr.

$$\frac{s_{opt}}{H} = C\left(\frac{W}{H}\right)(Gr\Pr)^{n} \tag{6.5}$$

6.2 APPLYING THE OPTIMIZATION PROCEDURE TO THE VARIOUS ASPECT RATIOS

Throughout the analyses of the different aspect ratios which are 0.5, 0.6, 0.75, 1, 1.5, 5, 10, and 15 analyses are conducted. Those results are introduced in Chapter 4. Remember that, the analyses are investigated for two parallel and vertical plates only. In this part of the study, results that is found in the analyses and introduced in the Chapter 4 extent to an array of vertical plates (i.e. the electronic package). This extension is done by using the procedure that mentioned in previous section. In summary; first, ‘‘$\dot{Q}_{total} H / WLk(T_{w,\max} - T_{\infty})$ versus s/H’’ graphs will plotted. Then, according to maximum values of $\dot{Q}_{total} H / WLk(T_{w,\max} - T_{\infty})$, optimum spacing between two vertical parallel plates is specified and then finally, ‘‘s_{opt}/H versus Gr x Pr’’ will plotted according to data which are found from the graphs of ‘‘$\dot{Q}_{total} H / WLk(T_{w,\max} - T_{\infty})$ versus s/H’’. Note that the ratios of optimum spacing to the plate height (s_{opt}/H) are placed on the ‘‘s_{opt}/H versus Gr x Pr’’ graphs.

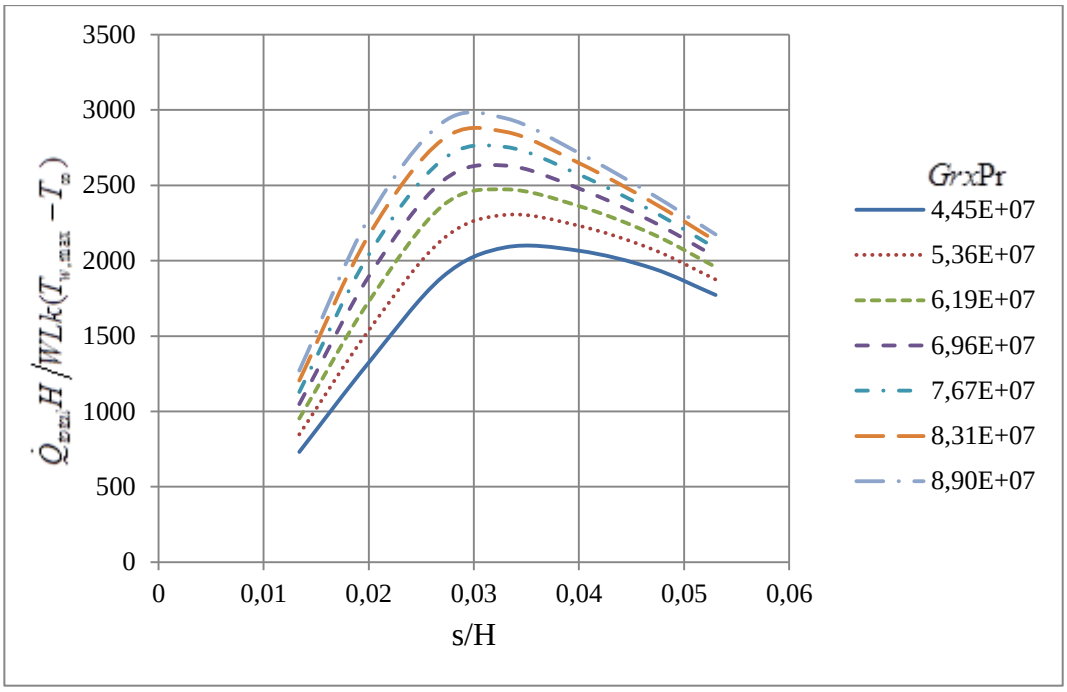

Fig. 6.1 Variation of Dimensionless Total Heat Transfer Rate with the Ratio of the Spacing to the Plate Height for W/H = 0.5

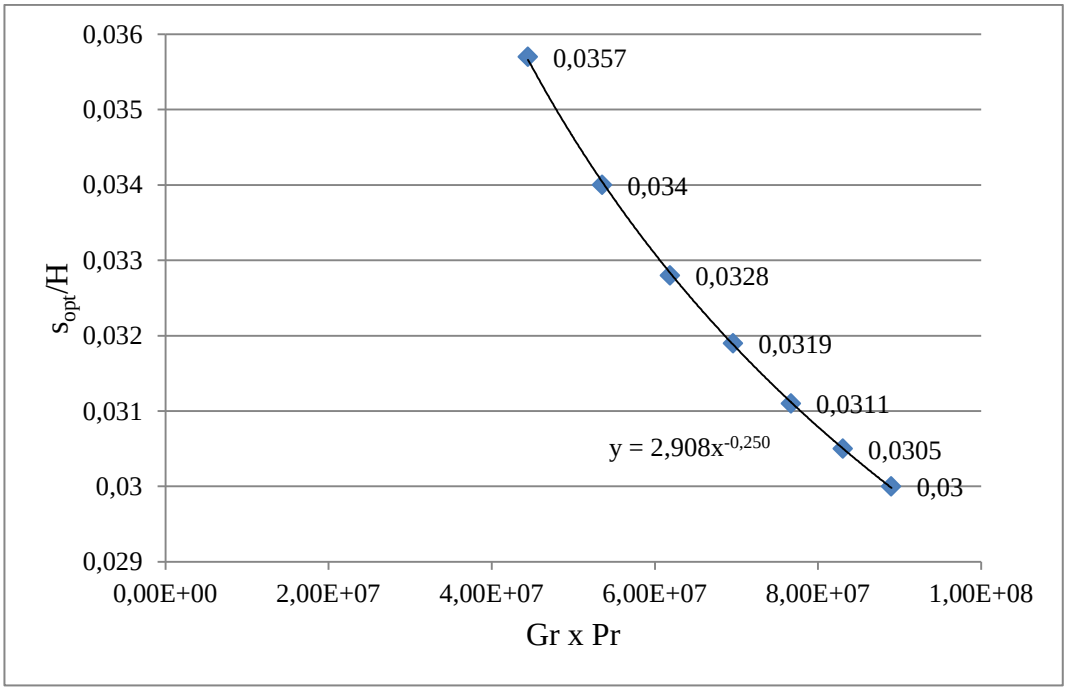

Fig. 6.2 Variation of the Ratio of the Optimum Spacing to the plate Height (s_{opt}/H) with the Dimensionless Group (Gr x Pr) for W/H= 0.5

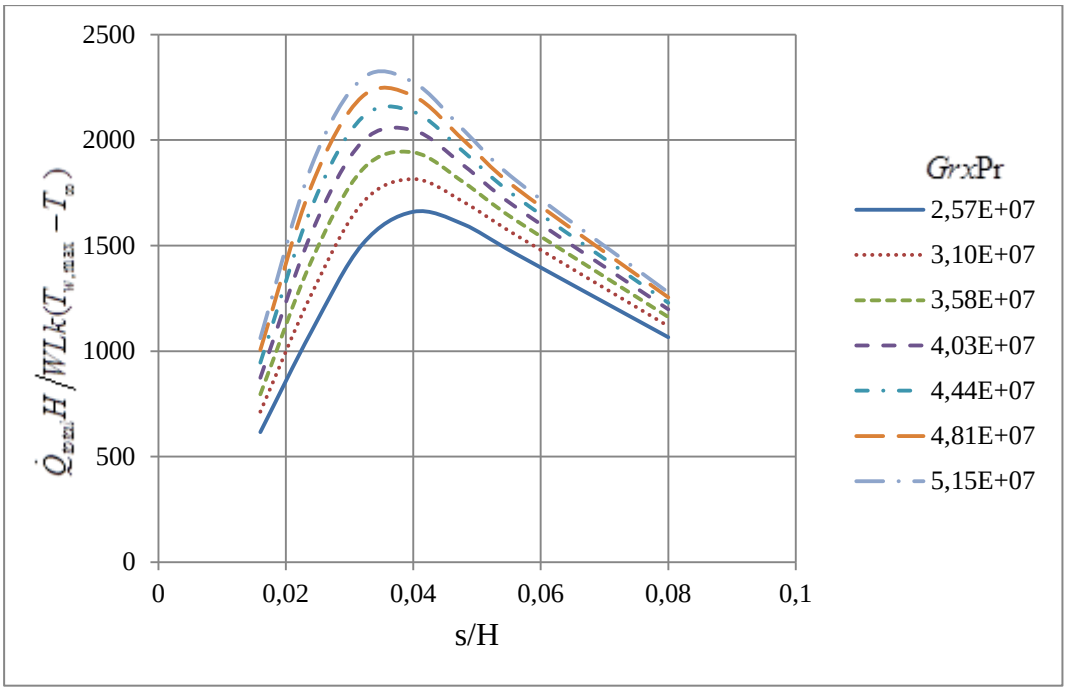

Fig. 6.3 Variation of Dimensionless Total Heat Transfer Rate with the Ratio of the Spacing to the Plate Height for W/H = 0.6

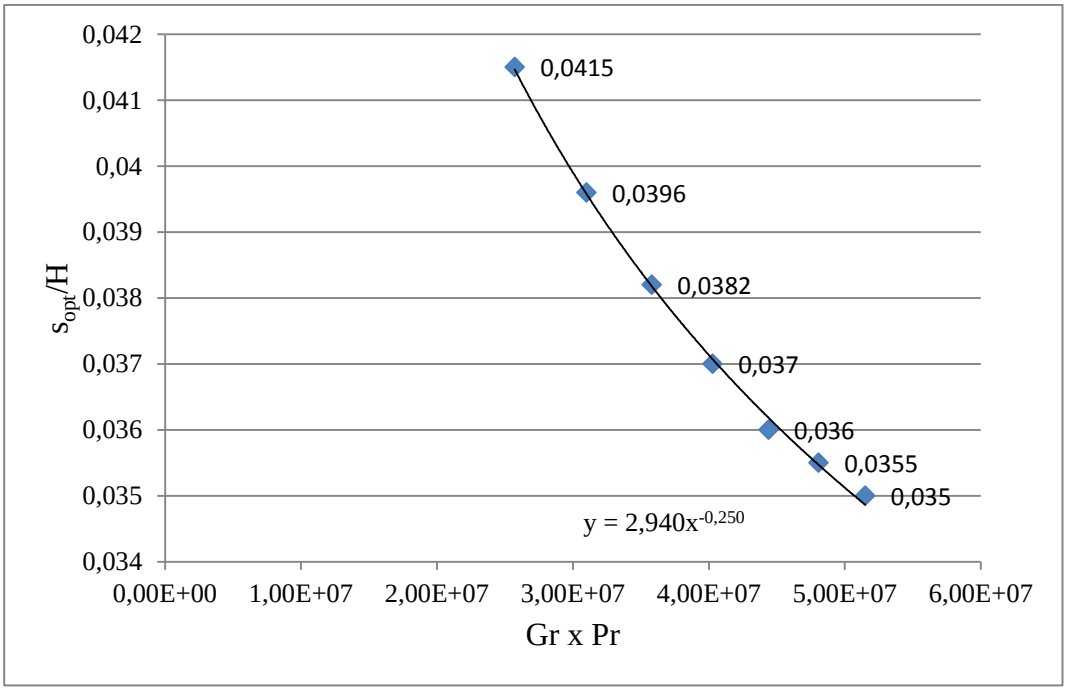

Fig. 6.4 Variation of the Ratio of the Optimum Spacing to the plate Height (s_{opt}/H) with the Dimensionless Group (Gr x Pr) for W/H= 0.6

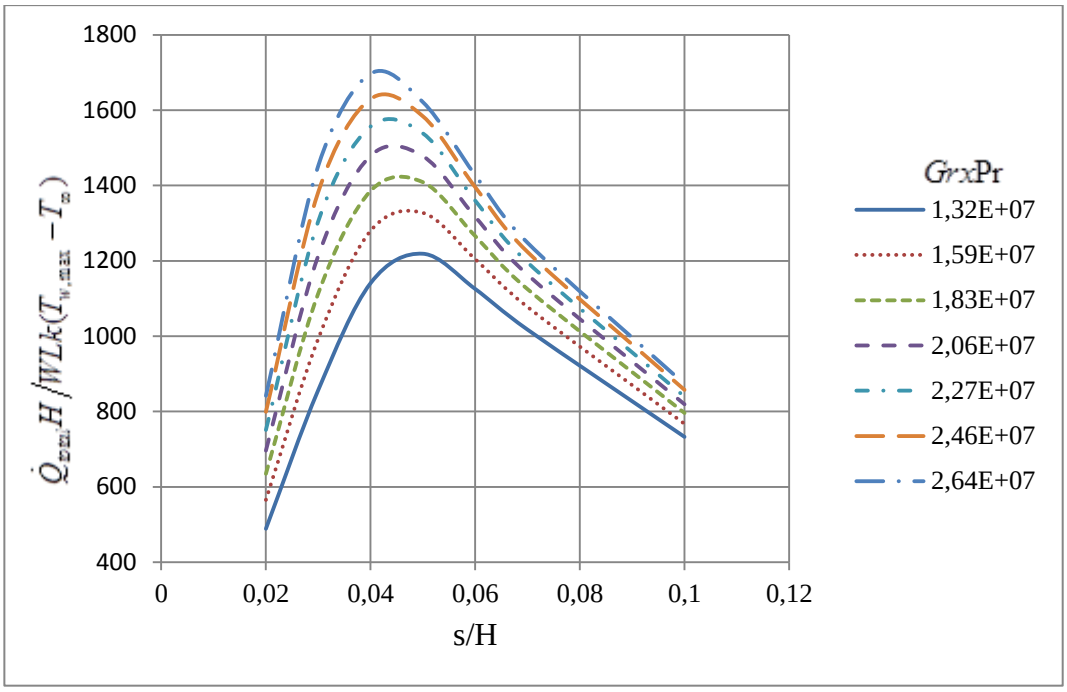

Fig. 6.5 Variation of Dimensionless Total Heat Transfer Rate with the Ratio of the Spacing to the Plate Height for W/H = 0.75

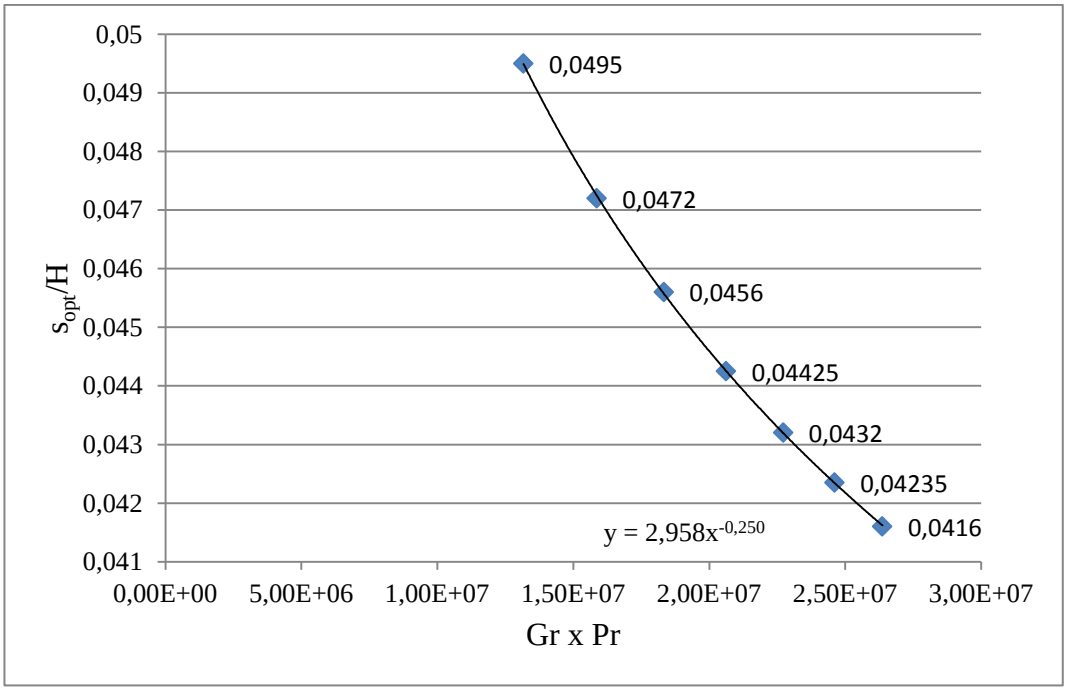

Fig. 6.6 Variation of the Ratio of the Optimum Spacing to the plate Height (s_{opt}/H) with the Dimensionless Group (Gr x Pr) for W/H= 0.75

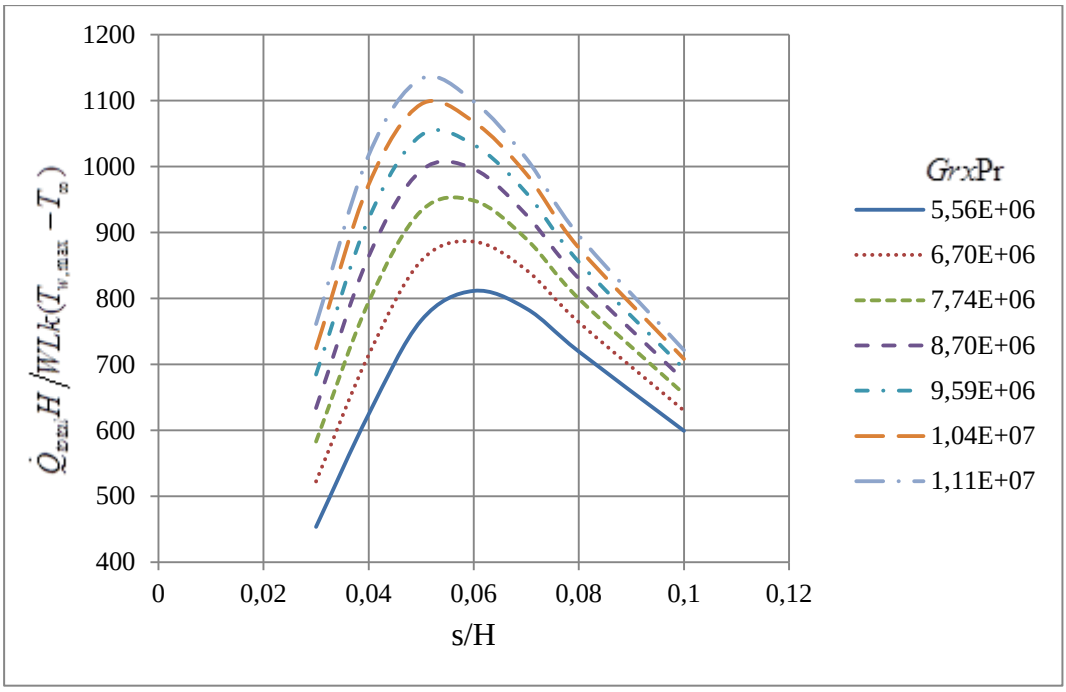

Fig. 6.7 Variation of Dimensionless Total Heat Transfer Rate with the Ratio of the Spacing to the Plate Height for W/H = 1

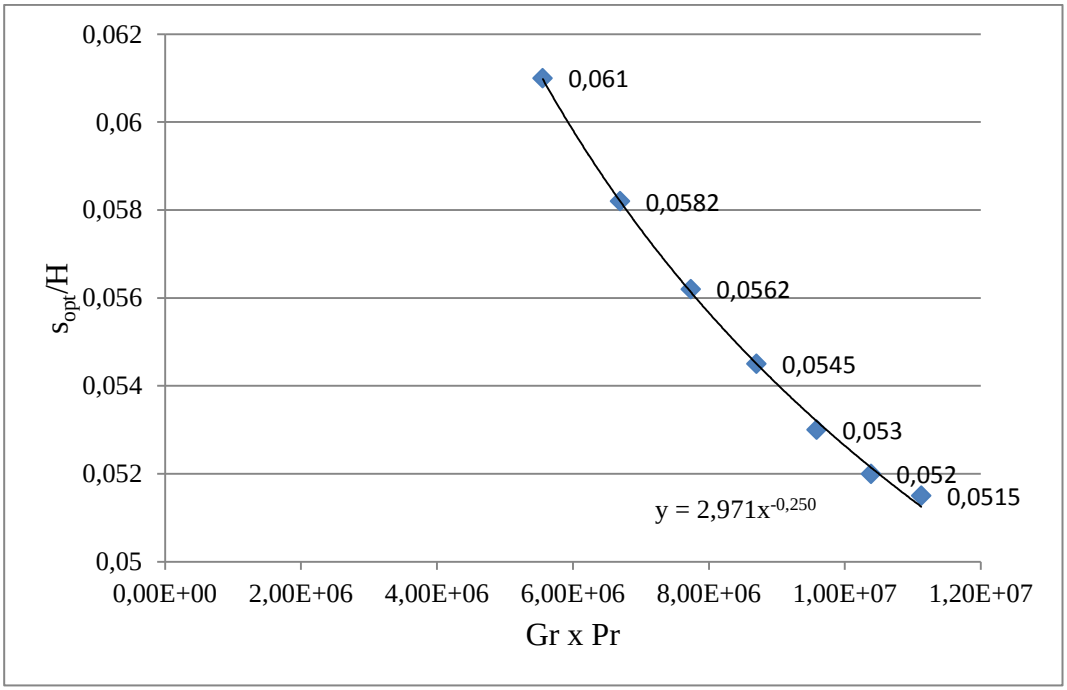

Fig. 6.8 Variation of the Ratio of the Optimum Spacing to the plate Height (s_{opt}/H) with the Dimensionless Group (Gr x Pr) for W/H= 1

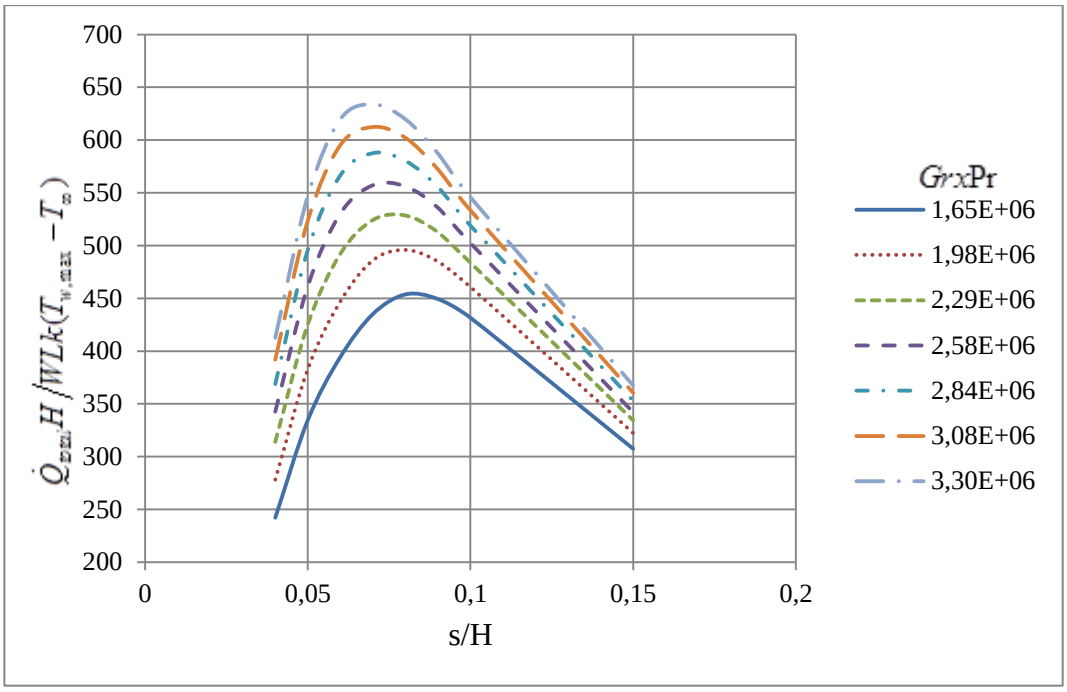

Fig. 6.9 Variation of Dimensionless Total Heat Transfer Rate with the Ratio of the Spacing to the Plate Height for W/H = 1.5

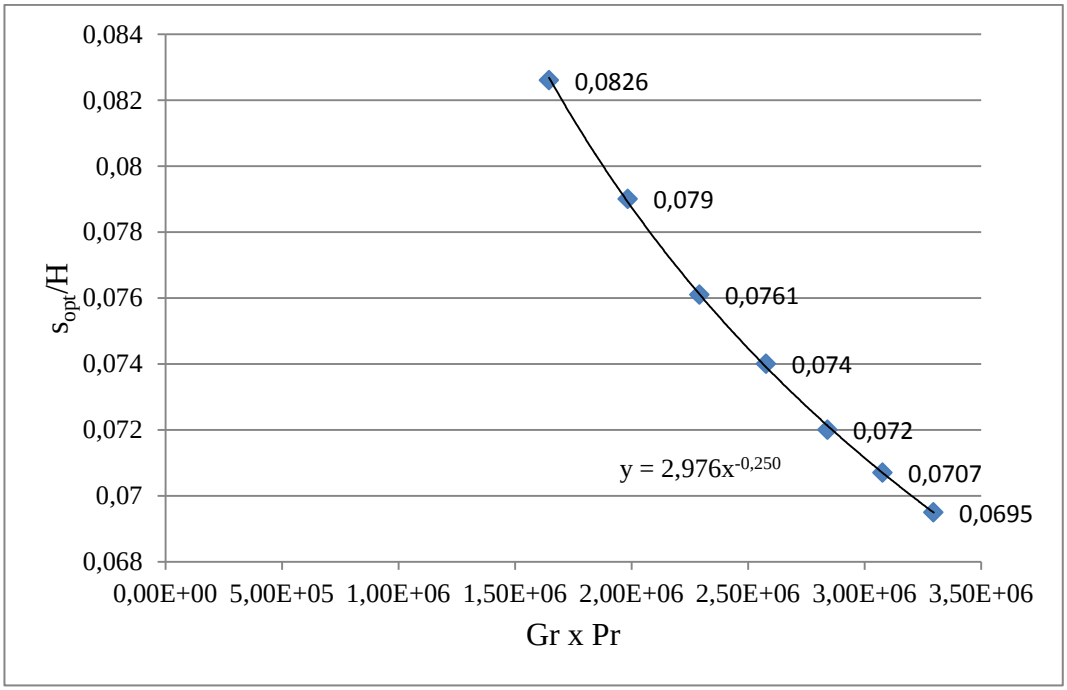

Fig. 6.10 Variation of the Ratio of the Optimum Spacing to the plate Height (s_{opt}/H) with the Dimensionless Group (Gr x Pr) for W/H= 1.5

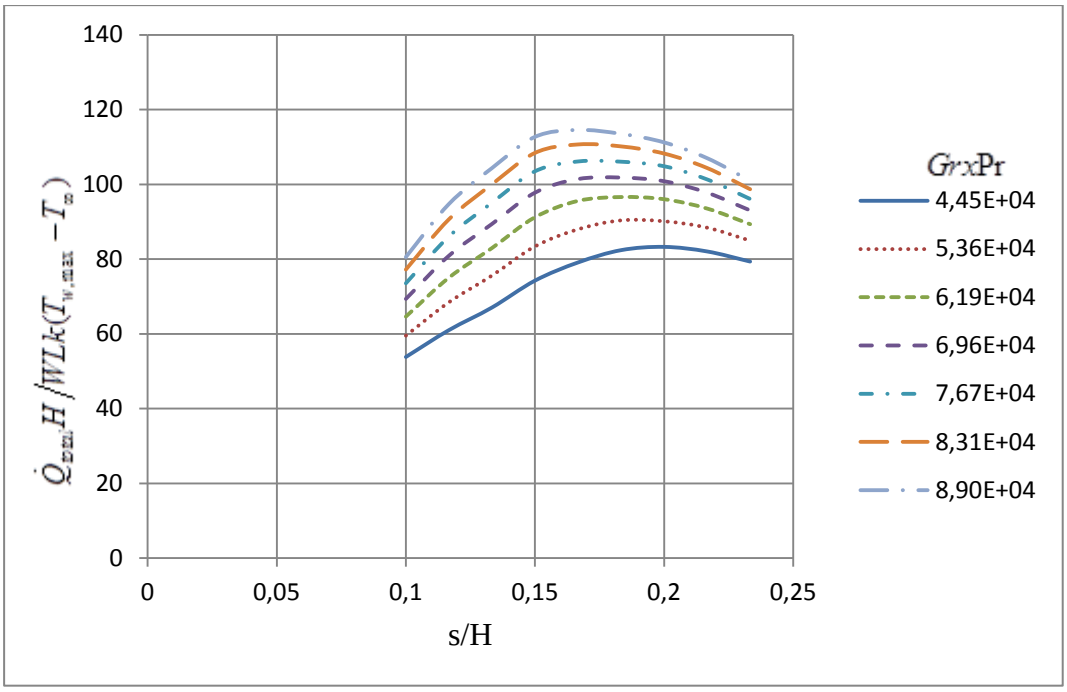

Fig. 6.11 Variation of Dimensionless Total Heat Transfer Rate with the Ratio of the Spacing to the Plate Height for W/H = 5

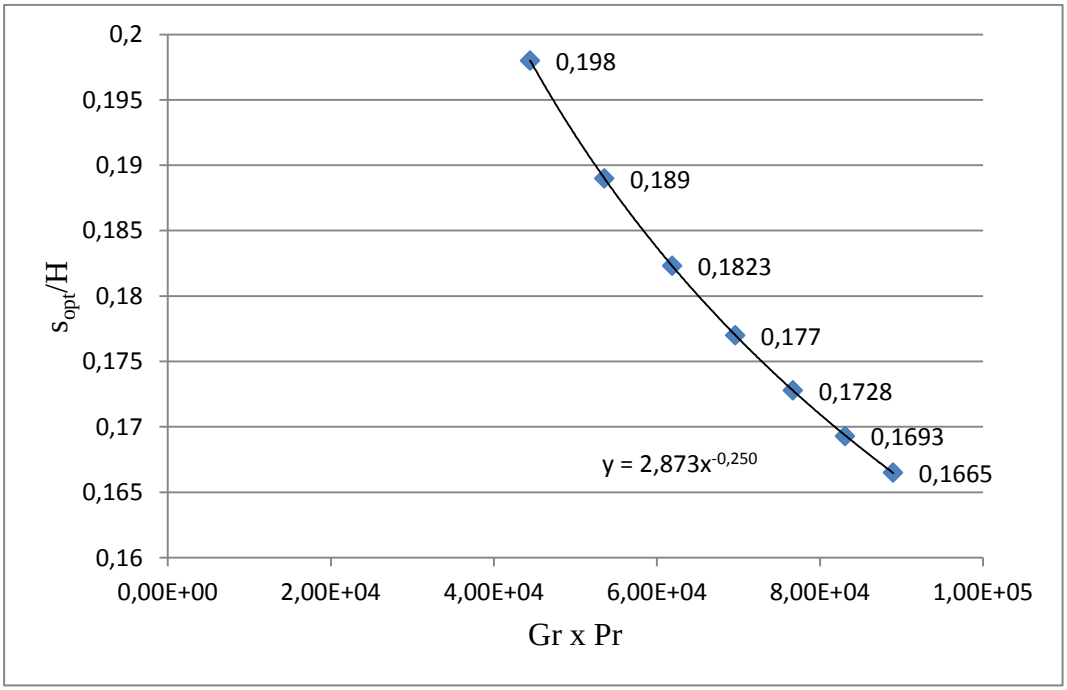

Fig. 6.12 Variation of the Ratio of the Optimum Spacing to the plate Height (s_{opt}/H) with the Dimensionless Group (Gr x Pr) for W/H= 5

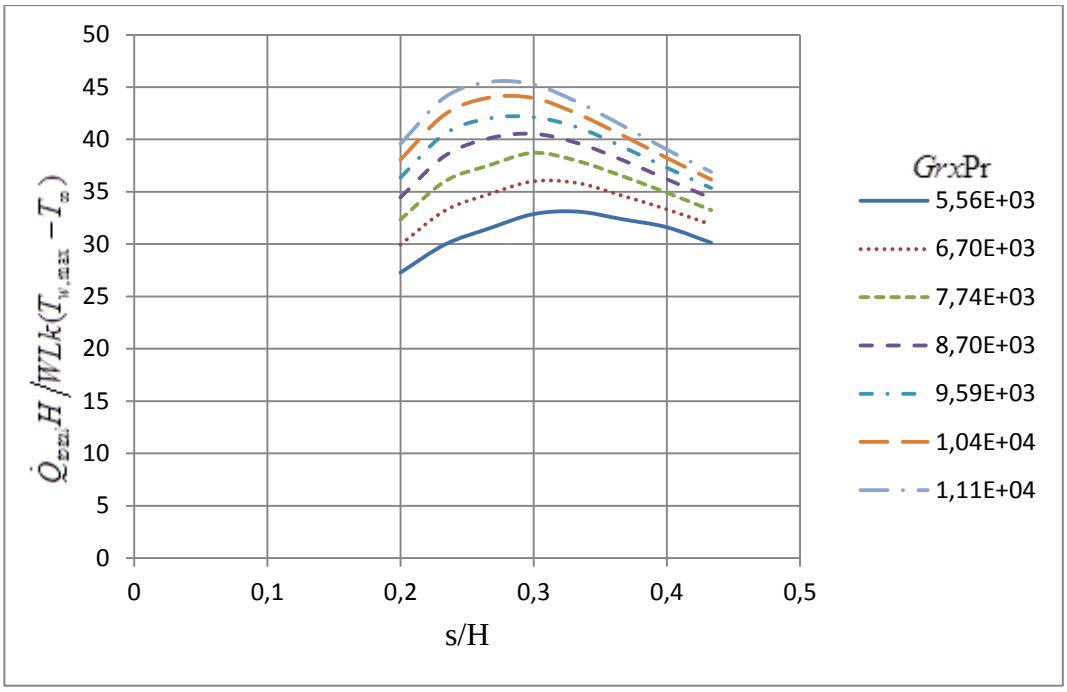

Fig. 6.13 Variation of Dimensionless Total Heat Transfer Rate with the Ratio of the Spacing to the Plate Height for W/H = 10

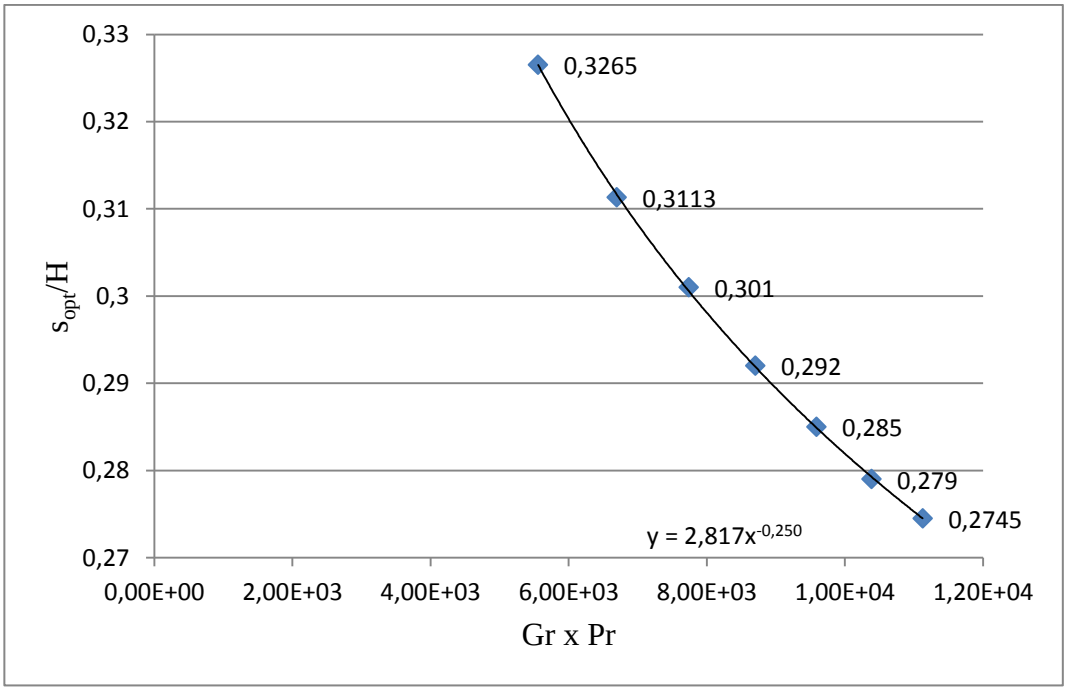

Fig. 6.14 Variation of the Ratio of the Optimum Spacing to the plate Height (s_{opt}/H) with the Dimensionless Group (Gr x Pr) for W/H= 10

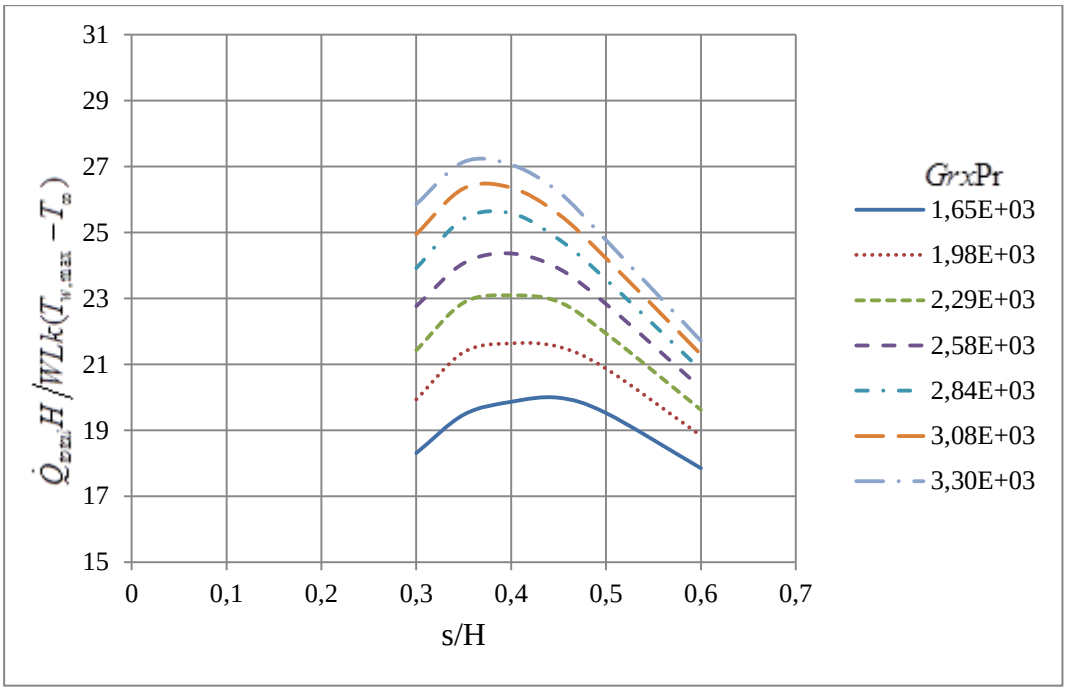

Fig. 6.15 Variation of Dimensionless Total Heat Transfer Rate with the Ratio of the Spacing to the Plate Height for W/H = 15

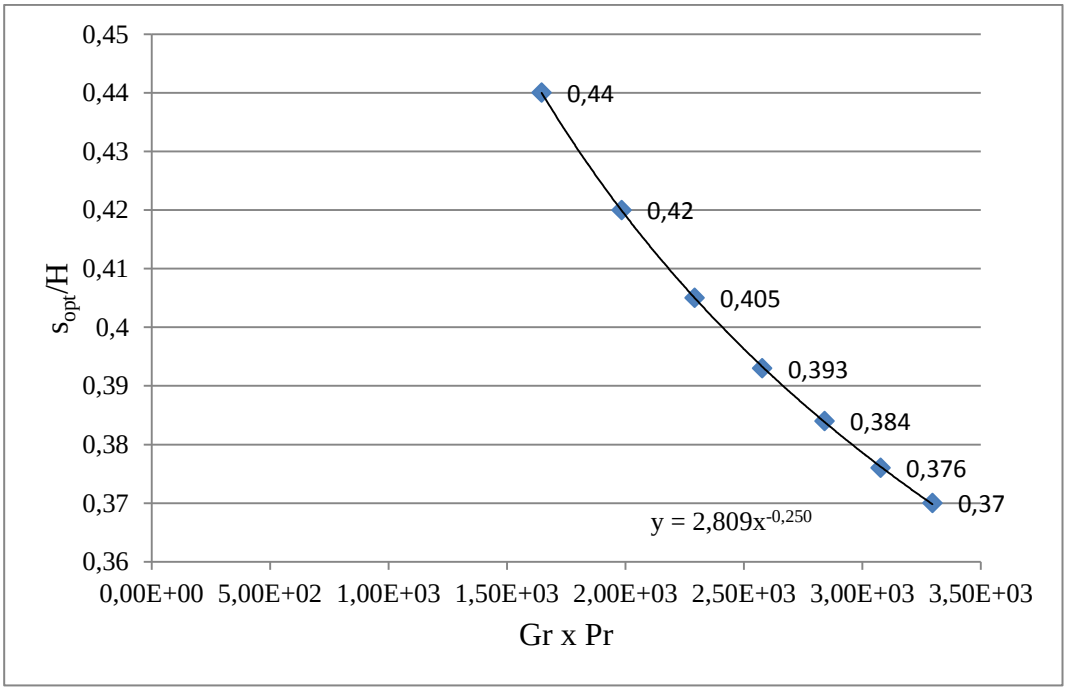

Fig. 6.16 Variation of the Ratio of the Optimum Spacing to the plate Height (s_{opt}/H) with the Dimensionless Group (Gr x Pr) for W/H= 15

6.3 RESULTS OF THE OPTIMIZATION PROCEDURE

The aim of the optimization procedure is to find a correlation between the ratio of the optimum spacing between plates in the electronic package to the height of the package (s_{opt}/H) and the dimensionless group (Gr x Pr) in the form of equation (6.7) where aspect ratio of the plates changes between 0.5 and 15.

$$\frac{s_{opt}}{H} = C\left(\frac{W}{H}\right)(Gr\,\mathrm{Pr})^{n} \tag{6.7}$$

In order to achieve that aim, a curve is fitted to all graphs of 9 different configurations which are showed the change of s_{opt}/H with respect to Gr x Pr (see Fig. 6.2- 6.4- 6.6- 6.8- 6.10- 6.12- 6.14- 6.16) by using MS Office tools. The results of the correlations for 8 different W/H configurations are listed in Table 6.1.

Table 6.1: List of C(W/H) and n Values for Different Aspect Ratios (W/H)

W/H	0.5	0.6	0.75	1	1.5	5	10	15
C(W/H)	2.909	2.940	2.958	2.971	2.976	2.873	2.817	2.809
n	-0.25	-0.25	-0.25	-0.25	-0.25	-0.25	-0.25	-0.25

The coefficients which illustrates the relation between s_{opt}/H and Gr x Pr are listed in Table 6.1. Note that the power of the dimensionless group (Gr x Pr) is same and equals to -0.25. Therefore, n is equal to -0.25 when the aspect ratio of plates (W/H) are between 0.5 and 15. On the other hand, the constant C(W/H) changes with changing aspect ratio (W/H).

In order to make the equation of optimum spacing more general, the variation of C(W/H) with respect to W/H is plotted in Fig. 6.19 by using the values that listed in Table 6.1. From the figure it can be seen that C(W/H) increases with increasing aspect ratio (W/H) where the aspect ratio is between 0.5 and 1.5. At W/H equals to 1.5, C(W/H) reaches its maximum value (2.976). Then it starts to decrease with increasing aspect ratio. When the aspect ratio equals to 15, the value of the C(W/H) is 2.809 and line becomes nearly horizontal (Fig. 6.17). Therefore, it can be said that when the aspect ratio approaches to infinity the value of C(W/H) is around of 2.8. The aim of this approach is to find a correlation for C(W/H) as a function of W/H. The possibility of writing this correlation will be discussed in Chapter 7. The results of Bejan and Lee [14] work show that C(W/H) equals to 2.3 when W/H approaches to 0. In the light of this investigation, the variation of C(W/H) with respect to W/H will be shown in Chapter 7.

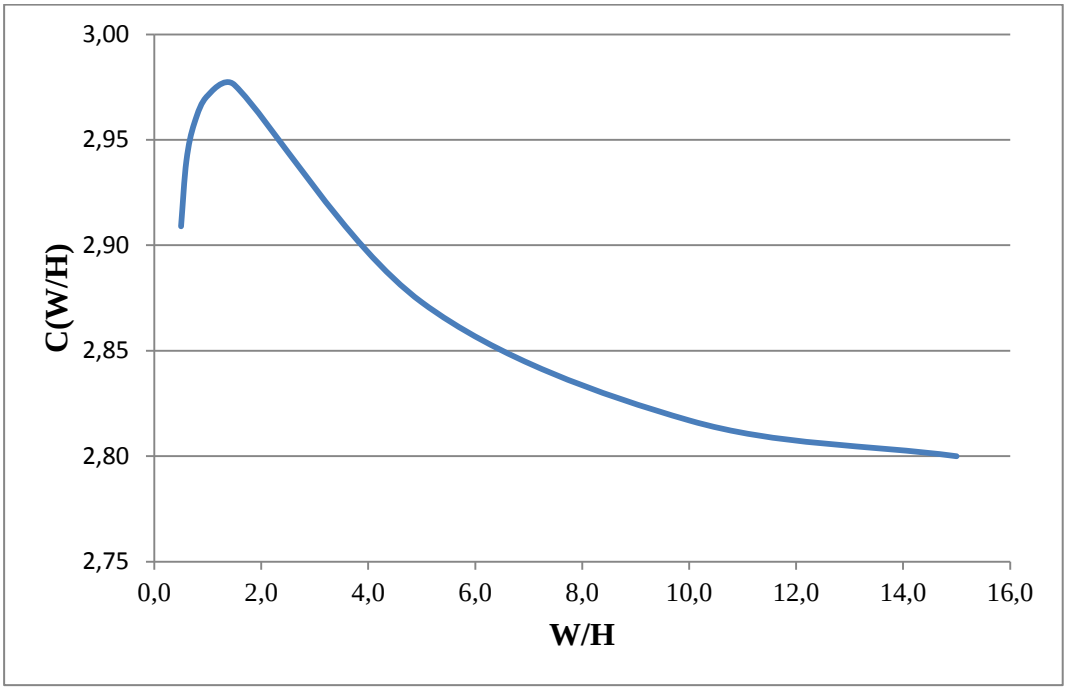

Fig. 6.17 Variation of C(W/H) with W/H

CHAPTER 7

DISCUSSION & CONCLUSION

Cooling of electronic devices is crucial for a reliable operating of those devices because of the allowable temperature limits of electronic components. Therefore, a proper cooling of those devices is an important issue for engineers. The aim of this thesis is to find an optimum spacing between array of vertical and parallel heat generating boards which are cooled by natural convection in a fixed volume. This array represents the electronic packages. In order to achieve this aim, first the heat transfer characteristics between two vertical and parallel plates for 8 different aspect ratios (W/H) under natural convection cooling were investigated numerically. The aspect ratio of the heat generating boards changed between 0.5 and 15 and the numerical solutions have been calculated by using commercial CFD software which is FloEFD. Secondly, these numerical solutions which were done for two vertical and parallel heat generating boards were extended to an array of boards for all aspect ratios in Chapter 6 and also in that chapter optimization procedure was applied to these arrays and optimum spacing between parallel and vertical heat generating boards under natural convection cooling was found in the form of equation (7.1). In the optimization procedure, first the variation of dimensionless total heat transfer rate $\left(\dot{Q}_{total}H/WLk(T_{w,\max}-T_{\infty})\right)$ was plotted with respect to s/H for constant Gr x Pr values. Then, from those graphs the value of s/H at the maximum dimensionless heat transfer rate was determined. Those values are called optimum spacing values (s_{opt}/H). Finally, according to those values, variations of s_{opt}/H with Gr x Pr was plotted for a specific aspect ratios and curve was fitted to those graphs. Those entire fitted curve was in the form of equation (7.1).

$$\frac{s_{opt}}{H} = C\left(\frac{W}{H}\right)(Gr\,\mathrm{Pr})^{-0.25} \tag{7.1}$$

Verifying the results of numerical solution is important in order to prove the reliability of the numerical solution. One of the ways of verifying the reliability of the numerical solution is performing experiments. Therefore, in this thesis an experimental setup was established for verification. In the experiments only one aspect ratio (W/H= 0.75) has been conducted and 4 different spacing were tested (s/H= 0.1, 0.075, 0.05, and 0.025). The dimensions of the fixed volume that was used in the experiment are 150 mm, 200 mm and 60 mm in width, height and length respectively. Setup, procedure and results of the experiments were showed in Chapter 5.

In order to compare the results of experiments and the numerical solution, first dimensionless heat transfer rate ($\dot{q}''H/k\Delta T$) was calculated for all 4 different spacing and various heat flux value. Then the variation of the dimensionless heat transfer rate ($\dot{q}''H/k\Delta T$) with respect to dimensionless group (Gr x Pr) was plotted in the same graphs for each spacing between the heat generating plates (Fig. 5.7-5.10). Those figures show that the results of the both numerical calculations and experimental studies have same trend. The maximum deviation occurs at s/H equals to 0.025 and the deviation is less for the larger spacings. There are several reasons that cause the deviation between the results of the numerical solution and the experimental study.

First of all, in the numerical solution, all lateral sides of the control volume assumed to be insulated. Although insulation material which has very low thermal conductivity (fiberglass) was used in the experiments, it is impossible to provide the fully insulated edges. Therefore, there are heat losses from the lateral edges and it affects the maximum temperature that occurs on the heat generating boards negatively. Secondly, in the mathematical model, uniform constant heat flux condition is modeled for the heat generating boards. In the experimental setup, in order to satisfy this boundary condition, heating spirals were used. Heating spirals

were wrapped around the plates 6 times. The distance between two heating spirals is approximately 1.8 cm for all plates. Although heating spirals are close to each other and the thermal conductivity of the copper plates is high, uniform heat flux condition cannot be satisfied perfectly. Therefore, it can be the one of the reasons of the deviation between the results of the numerical solution and the experimental study. Thirdly, the top and the bottom surfaces of the control volume are modeled as fully open to ambient in the mathematical model. However, in the experimental setup there are wires which provide the electrical energy to the plates in order to heat them is placed the right and left side of the plates at the bottom. Also, thermocouples are placed at the middle top of the plates in order to read the maximum temperature occurred at the plates. These are affects air flow of the system. Especially, when the plates becomes closer to each other (s/H= 0.025), the effects of these wires and the thermocouples on the maximum temperature that occurs on the heat generating boards increase. The prevention of the air motion from the bottom and the top edges of the channels increase the temperature of the plates. Thus, the deviation of the results between the numerical solution and experimental study is larger when s/H equals to 0.025. Finally, the effects of viscous dissipation become significant where the velocities are high. For example, viscous dissipation is taken account for the natural convection of the device which is rotating high speed. However, the heat generating boards that are used in this thesis are stationary. Also, the temperature difference between the ambient and the heat generating boards are in the order of 50°C at most. Therefore, maximum velocity due to the buoyancy force is low in the control volume. For those reasons, in the numerical solution of the problem, the effects of viscous dissipation were neglected. However, for the experimental setup, it is impossible to make the effects of viscous dissipation zero. Although the effect of viscous dissipation is small, it can be also one of the reasons of deviation between the results of numerical solution and experimental study.

In the [11], [14], and [20] the optimum spacing was written as a function of a coefficient and the dimensionless group (Gr x Pr) for natural convection cooling of parallel and vertical heat generating boards. The function that was found the

studies of [11], [14], and [20] has same structure of equation (7.1). In those studies the exponent of the dimensionless group (Gr x Pr) was found as -0.25. In this thesis, the exponents of the dimensionless group (Gr x Pr) for all aspect ratios are also found as -0.25. Therefore, there is a perfect consistence between those studies and this thesis for the exponents of Gr x Pr.

In this thesis, the aspect ratio of the heat generating boards changes between 0.5 and 15. The model of the study investigated by Bejan and Lee [14] is similar to the model of this thesis. However, the model that is used in the [14] was two dimensional. Therefore, Bejan and Lee [14] assumed that plates are very long with respect to its width; and the results of [14] are valid when the aspect ratio approaches to zero. The correlation which was found by the Bejan and Lee [14] is shown in equation 7.2.

$$\frac{D_{opt}}{H} \cong 2.3\left[\frac{g\beta(T_{\max}-T_{\infty})H^3}{\alpha\nu}\right]^{-1/4} \Rightarrow 2.3\left[Gr\,\Pr\right]^{-1/4} \qquad (7.2)$$

From equation (7.2), the coefficient equals to 2.3 in [14] when W/H is approximately zero. On the other hand, the calculated smallest aspect ratio equals to 0.5 and the coefficient equals to 2.909 in this thesis. However, from the Fig. 6.17, the value of the C(W/H) decreases sharply when the aspect ratio goes from 1.5 to 0.5. For example, the slope when the aspect ratio goes from 1.5 to 1 equals to 0.01. Then it becomes 0.052 for the aspect ratio is between 1 and 0.75. Between 0.75 and 0.6, slope becomes 0.12; and finally, it becomes 0.31 for the aspect ratio goes from 0.6 to 0.5. It shows that when the aspect ratio gets smaller the slope becomes larger in each step.

According to this trend of the variation of C(W/H) with respect to W/H, the value of the C(W/H) is estimated as 2.3 when the aspect ratio approaches to zero as in the study of Bejan and Lee [14]. This estimation is showed in the Fig. 7.1 with dashed lines. Although there are differences between the study of Bejan and Lee [14] and the current study, they support to each other when the general trend is

investigated. For example, the study of Bejan and Lee [14] was two dimensional and the effects of lateral edges to the performance of convective heat transfer are neglected. Bejan and Lee [14] also studied analytically. The small D-limit and large D-limit are used in order to specify the optimum spacing between heat generating boards. They also used the average heat transfer coefficient from the previous studies in the solution of the problem. On the other hand, in this thesis spacing values are investigated individually for all 8 different aspect ratio by using numerical method (finite volume method) and generalized for the array of heat generating boards. In summary, for the value of the W/H between 0 and 0.5, the dashed line in the Fig. 7.1 is used in order to determine the optimum spacing values. For the values of aspect ratio higher than the 0.5, the solid line can be used for the determination of optimum spacing values between the parallel and vertical heat generating boards.

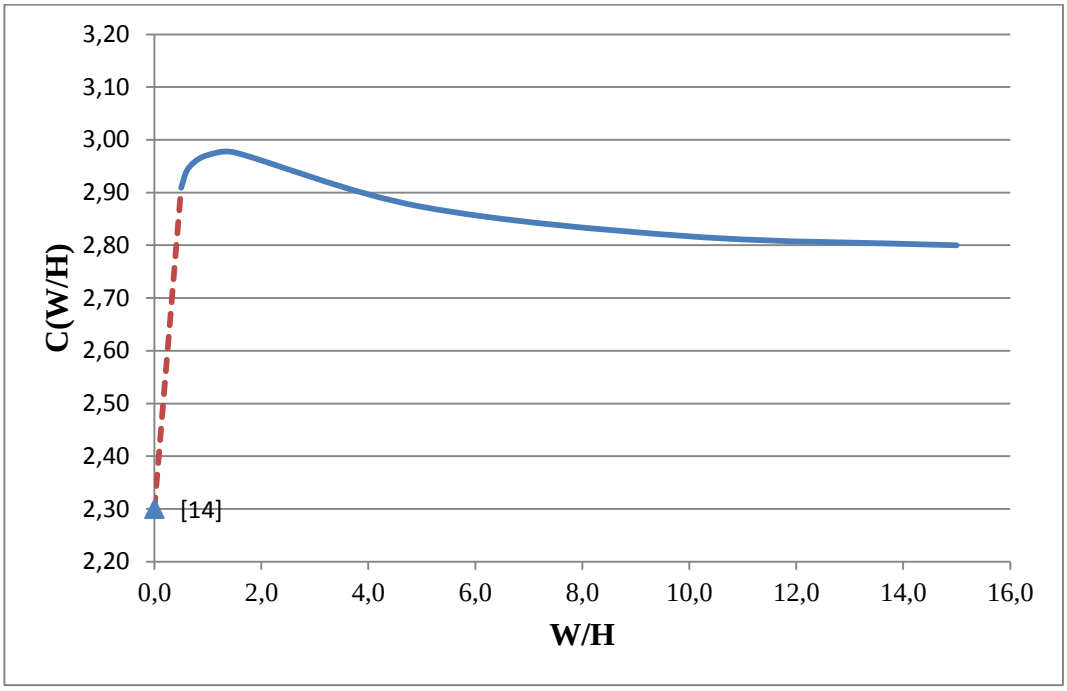

Fig. 7.1 Variation of C(W/H) with W/H (including W/H= 0 [14])

One of the aims of this thesis is to find the C(W/H) as a function W/H. In order to achieve this aim; the variation of C(W/H) with W/H was plotted in Chapter 6 (Fig. 6.20). From this figure it can be seen that, C(W/H) first increases with increasing W/H, and after a certain point (W/H= 1.5), C(W/H) decreases with increasing W/H. At around 2.8, C(W/H) is fixed with increasing W/H value does not affect the C(W/H). However, the smooth curve that was found in Fig. 6.20 cannot be written as a function of W/H. Therefore, instead of written a function of W/H, a coefficient (C) is defined and this constant is chosen from the Fig. 6.20. The function between the optimum spacing and the dimensionless group (Gr x Pr) can be written as:

$$\frac{s_{opt}}{H} = C(Gr\,\mathrm{Pr})^{-0.25} \tag{7.3}$$

In summary, in this thesis optimum spacing between two vertical and parallel heat generating plates under natural convection cooling is found as a function of Gr x Pr. The form of the equation is showed in equation (7.1). The study is done for Gr x Pr numbers between $1.65\text{x}10^3$ and $8.9\text{x}10^7$ when the aspect ratio changes between 0.5 and 15. From the plate dimensions and maximum allowable temperature increase a dimensionless group Gr x Pr can be calculated. The coefficient (C) value can be found from the Fig 7.1 since W/H is known from the plate dimensions. The rest of it is only calculation of the optimum spacing between two vertical and parallel plates in order to get maximum heat transfer rate at natural convection cooling.

To conclude, the finding of this thesis is important in some aspects. First, in this study convective heat transfer characteristics of parallel and vertical heat generating boards were investigated for various aspect ratios. Secondly, the heat transfer characteristics of two vertical parallel heat generating boards were extended to an array of heat generating boards. Finally, for this array of heat generating boards an optimum spacing between heat generating boards was found and formulized. Note that array of heat generating boards are very common for

many industry such as defense industry. For this reason the outcome of this thesis (equation (7.3) and Fig. 7.1) provides a proper decision for engineers about the spacing between two vertical and parallel heat generating boards under natural convection cooling.

REFERENCES

[1] Gürer A. T., Numerical Investigation of Incompressible Flow in Grooved Channels-Heat Transfer Enhancement by Self Sustained Oscillations, Ph. D. Thesis, ME Department of Middle East Technical University, 2004.

[2] Incropera F. P., DeWitt D. P., Bergman T. L., and Lavine A. S., *Fundamentals of Heat and Mass transfer,* John Wiley & Sons, Inc 2006.

[3] Kew P. A., Dunn, P. D., *Heat Pipes Theory, Design and Applications,* Oxford; Burlington, MA, Butterworth-Heinemann, 2006.

[4] Kakaç S., Introduction to ASI Cooling of Electronics, ,n Kakaç S., Yüncü H., and Hijikata, K., eds., *Cooling of Electronic Systems,* (cited in) Özdemir M. O., Optimum Design of Parallel, Horizontal and laminar Forced Convection Air-Cooled Rectangular Channels with Insulated Lateral Surfaces, M.S. Thesis, ME Department of Middle East Technical University, 2009.

[5] Kakaç S., Yaman Y., *Convective Heat Transfer,* Middle East Technical University, Faculty of Engineering, 1980.

[6] Bodoia J. R., and Osterle J. F., The Development of Free Convection Between Heated Vertical Plates, *ASME Journal of Heat Transfer,* Vol. 84, pp. 40-44, 1962.

[7] Sparrow E. M., and Bahrami P. A., Experiments on Natural Convection from Vertical Parallel Plates with Either Open or Closed Edges, *ASME Journal of Heat Transfer,* Vol. 102, pp. 221-227, 1980.

[8] Azevedo L. F. A., and Sparrow E. M., Natural Convection in Open-Ended Inclined Channels, *ASME Journal of Heat Transfer,* Vol. 107, pp. 893-901, 1985.

[9] Levy E. K., Optimum Plate Spacings for Laminar Natural Convection Heat Transfer From Parallel Vertical Isothermal Flat Plates, *Journal of Heat Transfer, Trans. ASME,* Series C, Vol. 93, No. 4, pp. 463-465, 1971.

[10] Levy E. K., Eichen P.A., Cintani W. R., and Shaw R. R., Optimum Plate Spacings for Laminar Natural Convection Heat Transfer From Parallel Vertical Isothermal Flat Plates: Experimental Verification, *ASME Journal of Heat Transfer,* Vol. 97, pp. 474-476, 1975.

[11] Ledezma G. A., and Bejan A., Optimum Geometric Arrangement of Staggered Vertical Plates in Natural Convection, *ASME Journal of Heat Transfer,* Vol. 119, pp. 700-708, 1997.

[12] Wirtz R. A., and Stutzman R. J., Experiments of Free Convection Between Vertical Plates With Symmetric Heating, *ASME Journal of Heat Transfer,* Vol. 104, pp. 501-507, 1982.

[13] Ramanathan S., and Kumar R., Correlations for Natural Convection Between Heated Vertical Plates, *ASME Journal of Heat Transfer,* Vol. 113, pp. 97-107, 1991.

[14] Bejan A., and Lee S. W., Optimal Geometry of Convection Cooled Electronic Packages, *Cooling of Electronic Systems,* Vol. 258, pp. 277-291, 1994.

[15] Anand N. K., Kim S. H., and Fletcher L. S., The Effect of Plate Spacing on Free Convection Between Heated Parallel Plates, *ASME Journal of Heat Transfer,* Vol. 114, pp. 515-518, 1992.

[16] Bar-Cohen A., and Rohsenow W. M., Thermally Optimum Spacing of Vertical, Natural Convection Cooled, Parallel Plates, *ASME Journal of Heat Transfer,* Vol. 106, pp. 116-123, 1984.

[17] Qing L., Suizheng Q., Guanghui S., Wenxi T., and Zhonghao Y., Experimental Research on Heat Transfer of Natural Convection in Vertical Rectangular Channels with Large Aspect Ratio, *Experimental Thermal and Fluid Science,* Vol. 34, pp. 73-80, 2010.

[18] Yüncü H., and Anbar G., An Experimental Investigation on Performance of Rectangular Fins on a Horizontal Base in Free Convection Heat Transfer, *Heat and Mass Transfer,* Vol. 33, pp. 507-514, 1998.

[19] Güvenç A., and Yüncü H., An Experimental Investigation on Performance of Fins on a Horizontal Base in Free Convection Heat Transfer, *Heat and Mass Transfer,* Vol. 37, pp. 409-416, 2001.

[20] Yazıcıoğlu B, and Yüncü H, Optimum Fin Spacing of Rectangulat Fins on a Vertical Base in Free Convection Heat Transfer, *Heat and Mass Transfer,* Vol. 44, pp. 11-22, 2007.

[21] Bejan A., *Convection Heat Transfer,* John Wiley & Sons, Inc., 1995.

[22] FloEFD for Creo 13.0 Technical Reference, © Mentor Graphics Corporation, 2013-12-07.

[23] Versteeg H.K., Malalasekera W., *An Introduction to Computational Fluid Dynamics, The Finite Volume Method,* Pearson Education Limited, 1995.

[24] IDEX Health & Science. Retrieved April 15, 2014, from http://www.idex-hs.com/materials/guide/delrin.aspx

[25] The Engineering Toolbox Retrieved April 15, 2014, from http://www.engineeringtoolbox.com/thermal-conductivity-d_429.html

[26] Revised Thermocouple Reference Table Retrieved April 20, 2014, from http://www.omega.com/temperature/Z/pdf/z223.pdf